Confocal microscopy

Chapter in Handbook of Comprehensive Biophysics (in press 2011) Elsevier

Brad Amos

MRC Laboratory of Molecular Biology, Hills Road, Cambridge CB2 0QH UK

e-mail ba@mrc-lmb.cam.ac.uk

Gail McConnell

University of Strathclyde , Centre for Biophotonics

161 Cathedral Street , Glasgow G4 0RE UK

g.mcconnell@strath.ac.uk

Tony Wilson

Dept. of Engineering Science, University of Oxford,

Parks Road, Oxford, OX1 3PJ, UK.

eMail: tony.wilson@eng.ox.ac.uk

Introduction

A confocal microscope is one in which the illumination is confined to a small volume in the specimen, the detection is confined to the same volume and the image is built up by scanning this volume over the specimen, either by moving the beam of light over the specimen or by displacing the specimen relative to a stationary beam. The chief advantage of this type of microscope is that it gives a greatly enhanced discrimination of depth relative to conventional microscopes. Commercial systems appeared in the 1980s and, despite their high cost, the world market for them is probably between 500 and 1000 instruments per annum, mainly because of their use in biomedical research in conjunction with fluorescent labelling methods. There are many books and review articles on this subject (e.g. Pawley (2006) , Matsumoto(2002), Wilson (1990)). The purpose of this chapter is to provide an introduction to optical and engineering aspects that may be o f interest to biomedical users of confocal microscopy.

Flying-spot Microscopes

A confocal microscope is a special type of 'flying spot' microscope. Flying spot systems were developed in the 1950s by combining conventional microscopes with electronics from TV and military equipment. Roberts and Young (1952) used a spot of light, scanned in a raster, on a cathode ray tube (CRT) as the illuminant for a transmission microscope image, which was displayed by scanning a spot on a TV screen in synchrony with that on the CRT, with a displayed intensity proportional to the output of a photocell (FIg 1). This system attracted some interest, particularly when a phosphor emitting ultraviolet light was employed, since the image showed absorption by chromatin. However, this was soon forgotten, because the image offered little advantage in resolution or contrast over a conventional (so-called 'wide-field') microscope.

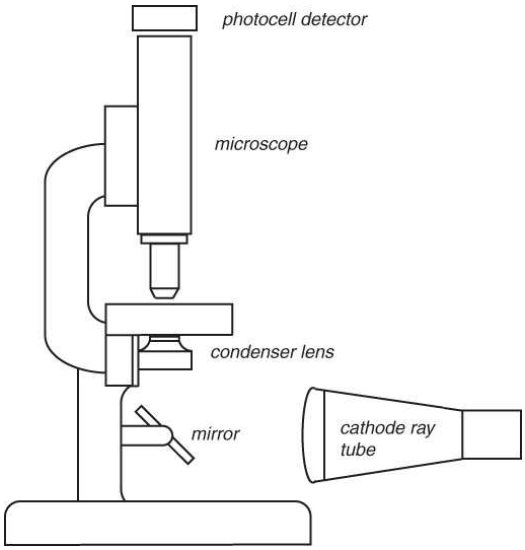

Figure 1. Flying-spot microscope of Roberts and Young: precursor of the confocal microscope.

It is, however, useful to consider here the advantages of the flying spot microscope, which were later exploited in a number of practical instruments and are relevant to current confocal microscopes.

First, there is a **low data rate**. The scanning of the specimen by a single spot of light , which is then received on a unitary detector such as a photomultiplier or photodiode, results in a single stream of data of relatively low bandwidth (typically less than 1 MHz) which is ideally suited to processing, using a computer. Early flying-spot systems, e.g. that of Freed and Engle (1962) used analogue computers, and this approach led to the production of commercial systems, culminating in a laser-scanning integrating interferometer (Smith 1972). Analogue to digital convertors are now used to allow modern confocal systems to construct the image in computer memory, to process and manipulate the image data and to drive the scanning and other systems.

Second, **multiple channels with precise co-registration** are easily implemented. This can be understood if it is imagined that a microscope as in Figure 1 is equipped with two or more detectors, each capable of picking up the emissions from differently-coloured fluorescent stains in the specimen. If the scanned spot of light included wavelengths that could excite all the stains, all detectors would be excited simultaneously if the spot flew over a specimen detail labelled with all of the stains. Provided the lens (the condenser in the Roberts and Young case) was achromatic, the detail would be shown as positive at an identical location in all the images. This is very difficult to achieve in non-scanning systems, for example with multiple cameras, since the cameras have to be held with single-pixel accuracy in equivalent positions in multiple images with identical magnifications.

Thirdly, **transmission imaging** in any of the conventional modes can be obtained simultaneously with epi-scanned images (i.e those in which the beam for excitation of fluorescence is delivered through the objective lens of the microscope and the same lens is

used for collection of the fluorescent emission). The transmission image merely requires pickup of all the light that passes through the exit pupil of the condenser lens (see below).

Fourthly, the **resolution of a flying spot microscope is determined entirely by the spot size of the illuminating beam**. If this is of short wavelength, but the detected emission is of longer wavelength (a phenomenon which invariably occurs in fluorescence and is termed the Stokes shift of wavelength) the resolution is that expected for the shorter wavelength.

A fifth advantage of the flying spot design over a conventional microscope is that, if a laser is used, a **very high intensity** of light can be concentrated in a spot which can be extremely small, ultimately at the limit of size set by diffraction. It was pointed out in a very prescient but obscurely-published paper by Sheppard (1980) that at the intensities obtained with lasers available at that time (megawatts per square centimetre, which may be compared with approximately 100 milliWatts per square centimetre for sunlight) nonlinear optical effects which are normally unknown on earth can be induced to occur. He obtained microscope images of mineral crystals emitting a second harmonic at twice the optical frequency of the flying spot illumination and suggested that if a pulsed laser beam could be used, the besetting problem of thermal damage might be mitigated. He also suggested that phenomena such as 2-photon imaging of the fluorescence of biomolecules might become possible. Ten years later, 2-photon imaging was achieved by the use of a femtosecond pulsed dye laser by Denk et al. (1990) and this was soon followed by the introduction of a femtosecond pulsed Titanium Sapphire laser for this purpose (Curley et al.). Webb and his colleagues found that in spite of the use of instantaneous powers approaching gigaWatts per square centimetre, the heating effect was indeed reduced to negligible levels by the pulsing strategy that Sheppard had suggested (see review by Denk & Svoboda, 1997). Apart from the confocal microscope, the nonlinear optical microscopes that are now used widely in biomedical research are the main surviving examples of the flying spot technology.

Confocal microscopes

Minsky, who was motivated by a desire to obtain three-dimensional information about the connections of neurones in the brain, designed, built and used a flying spot microscope of a special type in the 1950s (Minsky, 1998, for an account of his work in 1955). Minsky's crucial innovation was that the light scattered from the specimen was refocussed on to a small aperture and only the light that passed through the aperture was allowed to fall on the detector (Figure 2).

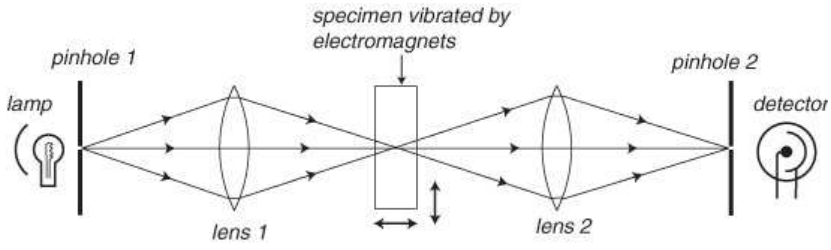

Figure 2. Minsky's scanned-specimen confocal microscope.

As with the microscope of Young and Roberts, the image was formed on an oscilloscope screen by intensity modulation of a spot scanning in a raster. Minsky pointed out that the use of the detector aperture gave the microscope an improved ability to discriminate depth. This type of microscope came later to be called 'confocal', because the source, the illuminated spot and the aperture leading to the detector were all at conjugate foci in the optical system (Sheppard & Choudhury, 1977). Like that of Young and Roberts, Minsky's microscope attracted little interest. It was unpublished except in the form of a patent application and may also have suffered because it was a transmission instrument and the depth discrimination of the conventional transmission microscope is so good (with depths of field of the order of 0.2 um, see Inoue (1989)) that there is no practical advantage in using confocal optics. Minsky's confocal principle showed its value only later when applied to fluorescence and reflection imaging. (Although one of Minsky's diagrams appears to show an epi-illumination microscope suitable for reflection or fluorescence, it actually represents a transmission system in which the transmitted beam was reflected back to the second pinhole by means of a mirror placed just after the specimen)

The invention of the laser stimulated a re-evaluation of the confocal principle (see historical reviews of the work of particular groups (e.g. Sheppard (1990) , Amos & White (2003) , and key papers in a published collection (edited by B.Masters (1996)) . This work laid the basis for an understanding of the optical principles of the confocal microscope and resulted in novel designs for the moving-stage scanning system, extensions of the confocal principle to interference microscopes, comparisons of the performance of microscope objectives in a confocal milieu and the development of methods of displaying confocal three-dimensional images . All of the early groups followed the Minsky design, in the sense that the specimen was scanned relative to stationary optics, with the advantages that the objective lens can be used to image on-axis, where its performance is best, and the size of the specimen can be increased almost indefinitely, provided the scanning system can contain it. These advantages were important in the examination of semiconductor wafers and other nonliving specimens, and led to the first commercial production of a confocal microscope in 1979 by Oxford Optoelectronics Ltd (Sheppard, 1990).

Confocal microscopes for biomedical use

The first impressive demonstration of the value of the confocal principle with biological specimens using stains with chemical specificity was that of Brakenhoff and his colleagues (1985): the 'optical sectioning effect' was clear in the images they obtained of fine particles within the nuclear chromatin of cells stained with fluorescent labels. This timely paper did not receive the attention it deserved, because of the insistence by the editors of 'Nature' that the title should emphasize the biological result and not the method of microscopy.

In 1981, the biomedical community had been galvanised by a conference at Cold Spring Harbor, where antibody methods had suddenly revealed beautiful structures termed 'cytoskeleton' within intact cells (e.g. Singer *et al.* 1982). Also highly selective fluorescent probes for calcium ions and other key physiological parameters had suddenly become available (Tsien *et al.* 1985). By the mid- 1980s, there was widespread use of fluorescent microscopes for studying these reagents but there was almost always, even in thin flattened cells, too much out-of-focus fluorescent structure for clear imaging. To give just one example, all mammalian cells round up before cell division, and clear images of the stages of division proved impossible to obtain. Improved depth discrimination was required: there was an urgent need for the development of confocal microscopes that were suited to biology.

Beam Scanning Confocal Microscopes

Carlssen and Aslund (1987), and slightly later White, Amos and Fordham (1987), developed laser-based confocal microscopes in which the specimen was left stationary and the beam was scanned over it. This was highly preferable in biological applications because the best objective lenses needed immersion oil in a thin film between objective and specimen, specimens were often in a mobile fluid such as water and living cells sometimes had to be impaled with a micropipette or electrode while being imaged. At that time, a flying-spot microscope was made available commercially, the Zeiss LSM 1, but it was not a confocal microscope: there was no detector aperture commensurate with the flying spot and it was merely an implementation of the laser-scanning flying spot systems that had been already been developed elsewhere over more than a decade (Schmidt et al. 1983).

The chief features of a beam scanning confocal microscope are shown in Figure 3. This Figure is intended to be generic: it applies equally well to the early systems of Carlssen et al. of White et al. and all the commercial systems up to the present, though it corresponds to none of these in detail.

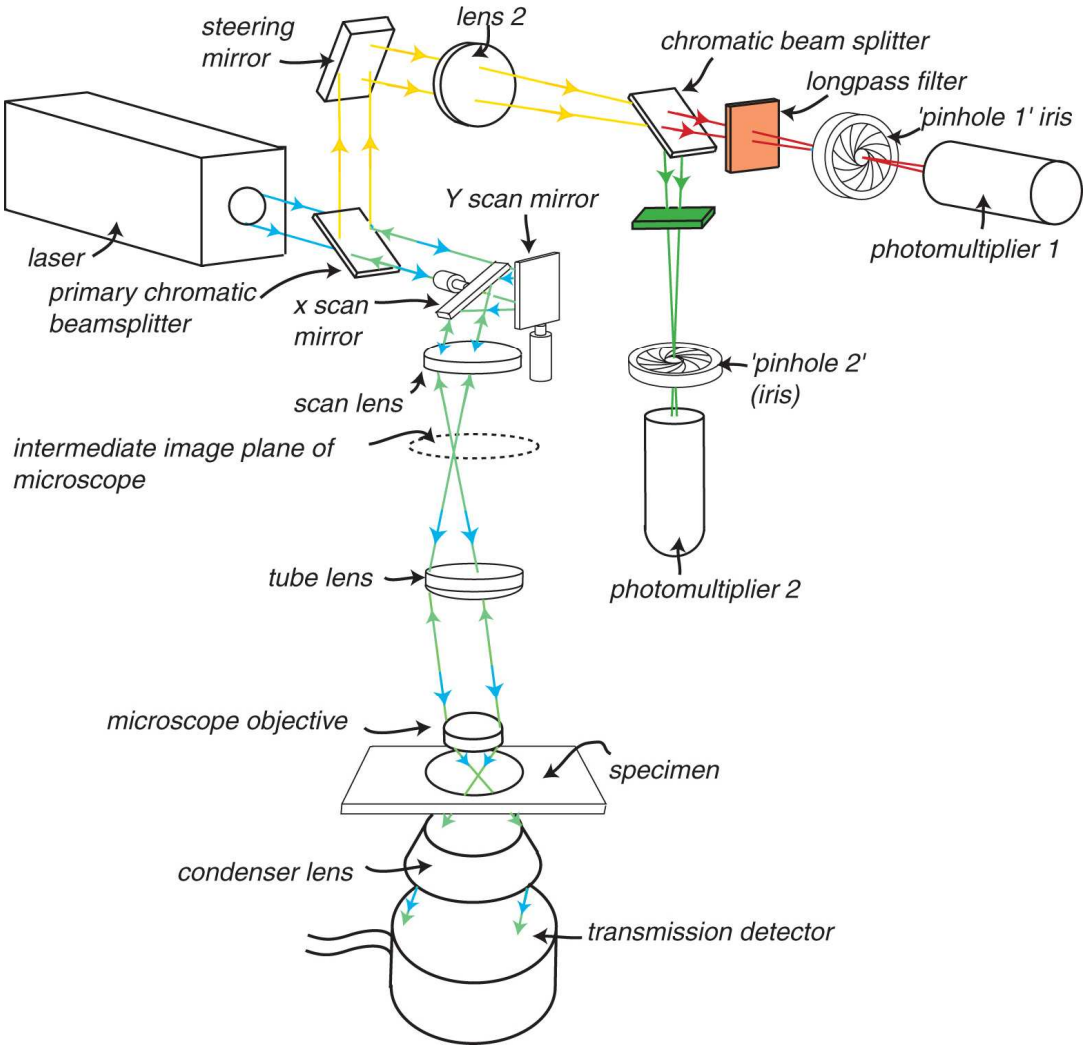

Figure 3 Generic beam-scanning single point confocal microscope. Light from a continuous (CW) laser passes through a primary beamsplitter, which allows a beam of a chosen set of wavelengths to pass to the scanning apparatus. In this drawing, there are simply two scan mirrors , imparting an angular scan in orthogonal directions, namely a slow (Y) direction and a faster (X). The scan mirrors are placed close to an aperture plane of a microscope system. It is a consequence of the basic geometrical optics of a microscope that aperture planes alternate with image planes throughout the system. In the aperture planes the laser beam undergoes a rotation without translation. In the image planes (intermediate image plane and specimen plane) there is a translation only. The laser beam is brought to a focus in the intermediate image plane of the microscope by means of a scan lens and then passes via a tube lens and objective to the normal focal plane of the microscope, where it is brought to a focus. It is essential for good resolution that the beam fills the back pupil of the objective at all times.

If light is scattered from the specimen, or is released by fluorescent molecules in the specimen, it proceeds back up the microscope tube and , in the short time needed to excite and release fluorescence the scanning mirrors have not moved appreciably. This causes the beam to be sent back toward the laser as a stationary beam. It would pass back into the laser, except that the primary beamsplitter may reflect a component (e.g. of wavelengths greater than that of the laser)

upwards, across the top of the diagram and into the detection system. An additional lens (lens2) focusses the emitted or reflected light on to a pinhole, (pinhole 1) which acts as a confocal detection pinhole. In the plane of the pinhole there is an enlarged image of the illuminated region of the specimen. The detector picks up light that passes through the pinhole. In the diagram a second detector and pinhole are also shown, with the signal light being divided between the two detectors by means of a chromatic beamplitter and a pair of appropriate barrier filters to isolate longer and shorter wavelength components of the signal beam.

At the bottom of the diagram the cylindrical object represents the wide-area detector which catches all the light emerging through the condenser lens. The function of this detector is to register the total beam power integrated over the entire aperture, which is a time-varying quantity which can be used to form a non-confocal transmission image, using any of the familiar transmission modes of the optical microscope such as bright field, phase contrast ,dark field or DIC. If care is taken to use the laser beam in a linear polarization of an appropriate azimuth, it is possible to form DIC and confocal epifluorescence images of maximum sensitivity simultaneously, since no analyzer need be placed in the body tube of the microscope and so attenuation of the epi-detected fluorescence can be avoided. |The transmission detector should be placed close to an aperture plane or equipped with a diffuser. If close to an image plane such as that of the field iris of the microscope it may itself be imaged obtrusively at the same time as the specimen.

The basic operation of such a system is described in the legend of Figure 3. It may now be useful to point out some of the special features which have been developed in particular implementations of the beam scanning design.

Starting at the laser, most modern systems do not have a direct light path as shown in Figure 3: they use a single-mode optical fibre to connect the laser to the scanning optics. Normally, several lasers are used, and an acousto-optic modulator is inserted between the lasers and the optical fibre in order to select which laser lines (wavelengths) are used . The acousto-optic device can be switched in a sub-millisecond time scale, allowing the same scan line to be followed by, for example, three lasers of different wavelength. This ‘wavelength strobing’ has the benefit of near-simultaneous imaging without the loss of spectral discrimination that occurs if all wavelengths are used simultaneously and only the emission is spectrally windowed.

In order to allow high-quality differential interference contrast imaging (DIC) the optical fibre has to be of the type which is designed to preserve the linear polarization state of the laser beam. Unless aligned with great care and protected from vibration and temperature changes, no fibre will do this, and ellipticity of the fibre output may produce serious faults in the image, ranging from microphonic disturbances (fine horizontal dark or light lines in the image) to a slow drift over tens of minutes. In the image, the retardance changes may be so great that the contrast , (e.g. darkness on one side of a subcellular object and light on the other) may be reversed.

The primary chromatic splitter determines the pointing direction of the stationary signal beam and, if replaced, must be repositioned with great precision. In the Bio-Rad 'Radiance' series of confocal systems it was replaced by an 80/20 beamsplitter that was not wavelength-selective which was fitted permanently in place. Suitable choice of input polarisation and reflection coating gave an 80% /30% split, with the greater loss applied to the laser beam, which in practice, always had power to spare. (Note that if the input beam is polarized at a suitable azimuth, the percentages do not have to add up to 100).

Scanning and Descanning the Beam

In an early prototype, a polygonal mirror was used to provide a fast scan (White,1987). This was abandoned because of the large translation (rather than pure rotational scan) of the output beam, a relatively poor duty cycle and the lack of precision in the interfacet angle of even the best polygons, which necessitated an optical indexing using a pilot beam to trigger the pixel clock of the electronic detection system. All current commercial systems use the 40 –year-old principle of oscillating mirrors driven electromagnetically by a mechanism similar to a moving iron or moving coil galvanometer, and termed ' galvo mirrors'. The best duty cycle for a given mirror (which means the largest fraction of the cycle spent in illuminating and collecting the emission) is obtained by driving the galvo mirror to follow a sawtooth curve when angle is plotted against time. This is demanding in power, particularly at high scan rates, and is limited to approximately 1 KHz oscillation frequency by the maximum rate of power dissipation in the drive mechanism, which is limited in spite of the provision of a heatsink. Higher frequencies, up to 8 KHz can be achieved by driving the galvo at a resonant frequency. If a bidirectional scan is used, the line scan rate can reach the 15 KHz of video images. This type of fast mirror scanning, essential for many physiological projects, was first achieved by Tsien (1995), who introduced the use of a pilot beam sweeping over a Ronchi grating for indexing of the fast sweep. Modern bidirectional scanning systems provide a user-accessible control for manual setting of the registration between successive scans, which can be set by observing a linear feature running vertically (i.e. in the slow scan direction) and adjusting the control to obtain a smooth line rather than a broken one, alternating in horizontal position in successive lines. Although resonant scanners are faster, they scan sinusoidally, so the spot slows towards the extremes of the scan, making only a central region usable, typically less than 1/3 of the total range. The poorer duty cycle has to be compensated by the use of higher laser intensities, if the same amount of emitted light per frame is to be collected as from a sawtooth scan.

The geometry of the optical microscope demands that the scanning be performed by a pure rotation of the beam in an aperture plane and this corresponds to a pure translation in the image plane, as required for scanning a specimen uniformly. In designing the precursor to the Bio-Rad systems White, Amos and Fordham chose to use a microscope eyepiece as the scan lens, since its aberrations are designed to minimise those of the objective and it is optimised to image the back focal plane of the microscope at a diameter of 1- 2mm in the so-called 'Ramsden disk'. The disk is the ideal position for the origin of the rotational scan and permits the use of a very small scanning mirror with a laser beam

of approximately 1 mm diameter. The focal length of the eyepiece was typically 32 mm, the mirror surface and axis of rotation had to be placed within a fraction of a millimetre of the Ramsden disk and a large scan angle (plus and minus 20 degrees optical , or 10 degrees mechanical) had to be used. This meant that if one mirror was placed correctly, the other gave an intolerable translation of the beam at the points where it ought to be stationary, i.e. in the Ramsden disk and in the back focal plane of the objective lens. White solved this by imaging one mirror on the other with a unit power refracting telescope. Amos replaced this with a pair of concave spherical mirrors which had the same function. Because of the small beam diameter the performance of this cheap and simple optical relay system was remarkably high, showing no aberrations even with full-field scans of 1000 x 1000 pixels. Recently, this arrangement has b een improved by the use of non-spherical mirrors (Sharafutdinova et al. 2009) . The high-angle eyepiece-based scanner was ideal in a system which had to interface with microscopes from many different manufacturers, where the only change necessary was the substitution of the appropriate eyepiece and an alteration of the distance between the closer mirror and the eyepiece to suit the two-fold variations in the height of the Ramsden disk in different optical systems. This made it easy to adapt the successive scan head models manufactured by Bio-Rad to different microscopes.

Current manufacturers, who have no interest in accommodating their confocal scanning apparatus to the microscopes of their rivals, have all taken a different approach. Instead of an eyepiece, a lens of 100mm or greater focal length is used and the lens-to-galvo mirror distance is fixed. This makes the scan angle at least 3x smaller and the beam size on the mirror 3x bigger, but reduces the error due to axial displacement of the galvo mirror so that the two mirrors can simply be mounted in close proximity to each other, without any optical relay to focus one on the other. This is called the 'close coupled' arrangement. If the beam is arranged to be slightly overfilling the back aperture of the objective, the fact that it is not perfectly stationary does not affect the resolution of the scan. The only effect on the signal beam is that it is in slight translatory motion throughout the parts of the signal path that are stationary in the ideal system, but the image formed at the level of the confocal aperture is perfectly stationary, though formed by a beam that is constantly changing slightly in angle. This non-ideal configuration has been found to work quite acceptably in practice.

The simplest and optically most perfect solution is to mount a single mirror in a gimbal arrangement so that it can perform scanning oscillations in two orthogonal directions. This 'cardanic' arrangement was used by Leica, but has now been abandoned in favour of the more conventional two-mirror system. Other current variations include the use of four close-coupled galvos linked by exchangeable beam-steering chromatic reflectors (Nikon), which allows the simultaneous use of two independent scanners within the same optical beam, acting on light of different colours. Thus it is possible to scan continuously and image with a beam of one wavelength before, during and after a short pulse to a scanned region of interest delivered at another wavelength.

Other geometrical solutions to achieving a near-invariant scan origin by the use of two mirrors depend on having one of the mirrors oscillating about an axis far from the

beam position on its surface (see Stelzer, 1995 for diagrams of various arrangements). This can produce a spot which is almost stationary on the second mirror. However, there is a strong incentive to keep the two mirrors mechanically identical, since, if this is done, the slow mirror can be driven fast and vice-versa, which rotates the scan through a right-angle, and suitable electronic drive signals can produce any desired rotation of the scan raster. This is incompatible with the commonest current Leica mirror arrangement, so an alternative is provided in the form of a conventional roll prism of the Abbe-Koenig or 'K' prism type, which causes the scan to rotate through twice the angle through which the prism is rotated around the optical axis. Scan rotation is required not just for positioning specimens in an aesthetically pleasing frame, but to arrange the fast scan along the best axis for certain types of experiment, such as observing events on an elongated neuronal axon as nearly simultaneously as possible.

Non-galvo scanners

Confocal microscopes have also been made with non-mirror scanners. Goldstein *et al.* (1990) used an acousto-optic scanner to achieve very rapid scanning. The chief difficulty of this scanning mechanism is that it is basically an optical phase grating formed by sound waves in a transparent material, and, like all gratings, gives dispersion of colour, which prevents the accurate aiming of the return signal on to the confocal detector aperture. Goldstein's solution to this problem was to revive a little-known device from the history of television cameras, known as an 'image dissector tube', which converted the optical image in the returning light on a photocathode into a coherent electron image which could be scanned electrostatically over an aperture at video speeds or higher. Draajer and Houpt (1988) adopted the simpler approach of working purely with light, but using a slit instead of a circular detector aperture, so that the polychromatic signal beam was not descanned by the acousto-optic deflector at all but merely passed up and down the slit, which served as a confocal aperture. Surprisingly, the images from this type of confocal microscope had no detectable anisotropy in spite of the use of a slit. Although promising results were obtained with a prototype acousto-optical confocal microscope (Oldenburg et al. 1993) mirrors have remained the scanning method of choice, probably because of their low cost and achromatic behaviour. The problem of designing an achromatic acousto-optic scanner is being solved currently in the group of R.A. Silver (Kirkby et al. 2010) but has not been applied to confocal microscopes as yet and is likely to be costly.

The confocal microscope has provided many challenges to the microscope makers. One is the need for improved chromatic performance in objective lenses, since the axial discrimination of the confocal system reveals longitudinal chromatic aberration that would be unnoticed in a conventional microscope. 'Violet corrected' objectives have been developed, so that fluorescent stains which are excited by near- ultraviolet radiation (such as DAPI) are seen in their correct location in a three-dimensional confocal dataset, instead of displaced towards the objective relative to visible-range fluorochromes.

Confocal Imaging at Different Wavelengths

Much effort has gone into the spectral aspects of detection in confocal microscopes. The scheme in Figure 3 represents that of the early Bio-Rad/ MRC systems, in which a chromatic beamsplitter was used to separate the emission beam into two spectral components, using a unit resembling a Ploem cube (see Herman & Tanke,1998) except that it contained two barrier filters and two beams emerged from it, entering two different detectors via two independent detector apertures. Later models from the same manufacturer added a third detection channel.

The fact that the descanned signal beam in a confocal microscope is well-collimated and stationary makes it easy to implement a grating or prism spectrograph in the emission path, and improve the flexibility of the spectral windowing of the emission. However, there is a serious problem, in that the incident laser beam is invariably reflected back into the detector system with an intensity many orders of magnitude greater than that of the fluorescent emissions. The prism or grating systems used in confocal microscopes have to be equipped with carefully and actively positioned opaque fingers or baffles, to prevent the laser beams from swamping the desired signals. Leica have implemented a robust and popular spectral system using a prism followed by motorised baffles to isolate a number of different segments of the spectrum. This system contains only a single variable detector aperture which serves for all wavelengths. A chronic controversy has existed between the defenders of this system (which cannot have the correct diameter of aperture for all wavelengths) and those of the Bio-Rad/MRC design, where the multiple apertures allow the setting of the aperture correctly for wavelength, or, more controversially, a balancing of signal strength even when the signals are vastly different in intensity by opening one aperture more than another. This has the effect of changing the optical sectioning depth in the different channels (see below). A design has been suggested (Amos, 2003) which combines the flexibility of the Leica spectral separation with the multiple apertures of the Bio-Rad system. Zeiss and Nikon use a multicathode photomultiplier in conjunction with a holographic grating to increase the number of spectral channels to 32. This allows rapid and detailed spectra to be obtained, and spectral unmixing algorithms have allowed the discrimination of objects in the microscope field even when there is some spectral overlap in emission and simple windowing with a spectrograph or filter system cannot separate them. The multicathode approach is not without drawbacks however. The gain is the same for all channels, which means that the dynamic range of detection is reduced. Also, the use of a grating causes an undesired loss of components of the signal beam linearly polarized at right angles to the bars of the grating. This is lessened in the Nikon systems by a prismatic polarizing rectifier which rotates the plane of polarization of the incorrectly polarized component of the beam before sending it over the grating.

There is little doubt that more ideas from the field of spectroscopic instrumentation could be incorporated into confocal microscope systems. The collimated beam is ideal for interferometry, and spectroscopy in the Fourier domain has been considered but not implemented commercially. Buican & Yoshida (1992) have suggested the use of a photoelastic birefringent crystal, oscillating through many cycles of path difference during each pixel dwell time. Dixon and Amos (2005) proposed a simpler but

slower system involving the use of a polarizing interferometer in the emission beam and the acquisition of a series of images, from which an interferogram could be derived for every pixel and, by inverse Fourier transformation, a spectrum for each pixel with a resolution determined by the number of images acquired. This could be incorporated easily into existing systems.

The Detector Aperture

The final step in the confocal process is the passage of the signal light through the detector aperture. A convenient feature of the design of White (1987) , was the use of extra magnification in the emitted light path, which meant that a diffraction limited spot was magnified (see below) to such an extent that it could fill an aperture of millimetre dimensions in front of the detector. The confocal aperture could then be simply a photographic iris, the diameter of which could be varied easily. This simple feature made for easy adjustment and cheap manufacture. In spite of the success of this system, marketed by Bio-Rad, initially as the 'MRC 500', all current manufacturers have persisted with the older notion of a microscopic aperture. The appropriate aperture size is determined by the magnification in the path from the intermediate image to the image in the plane of the aperture. In Figure 3, this would be the focal length of the lens L2 divided by that of the scan lens. In the Bio-Rad MRC 500-1024 systems the extra magnification factor was approximately 70, and in the Bio-Rad Radiance series it was 90. It can be calculated from information provided by Leica that their factor is approximately 5, and a similar factor is presumably present in all the other non-Bio-Rad systems, since they all use microscopic apertures. Since the extra magnification factor is shrouded in secrecy, the user is obliged to trust the on-screen indication of the pinhole size in Airy Units, now provided, calculated from the secret factor and the magnification and numerical aperture for each objective. The continued use of variable microscopic apertures operated by piezo mechanisms is surprising, since they must be expensive to manufacture and sensitive to contamination. There has been competitive argument about the merits of their exact shape, since the earlier ones were square. In practice, the departure from circularity has never been shown to affect the image, probably because the instrument response is determined by a multiplication of the illumination function by the detection function, rather than by a convolution, such as is seen in an out-of –focus camera image, where the shape of the camera iris may be clear and obtrusive (see below).

Optics of the confocal single-point scanning microscope

To a beginner, the images of very tiny isolated objects such as fluorescent bacteria or fine filamentous subcellular organelles or small light-scattering particles in the confocal microscope resemble those in a conventional microscope. The real difference is in the imaging of larger objects such as whole cells, embryos or tissue fragments, where a clear optical section is seen, devoid of glare from out-of-focus structures. In epifluorescence or epireflection mode, the confocal image is dark if the specimen is even slightly out of focus.

A simplistic ray-optical explanation of this is that the illumination in a single-point confocal system is in a cone of light, so the intensity falls off according to an inverse square rule with distance from the focal plane. At the same time, because of the pinhole, the detection efficiency also falls off, also with an inverse square rule, so the image intensity, which is a product of illumination intensity multiplied by detection efficiency, obeys an inverse fourth-power rule. This explains the optical sectioning effect but fails to account for the resolution effects near focus which are a consequence of wave optical behaviour. For a more rigorous account, classical resolution theory can be applied, but there is still some confusion about the optical sectioning, where both ray optics and physical optics must be combined. In this section, equations will be given without explanation, using real units rather than the optical units that are so convenient for making general calculations. Optical units are defined and used in the Appendix, where an attempt is made to explain the form of the equations.

The symbols and abbreviations used here have the following meanings:

n refractive index of the immersion medium

λ vacuum wavelength (excitation or emission wavelength will be specified where appropriate)

NA numerical aperture of the lens (= $n \sin \alpha$, where n is refractive index and α is the angle to the optical axis of any ray that enters the objective lens at the edge of the entrance pupil of the lens (i.e. the maximum possible angle for a ray that contributes to the image).

FW Depth of field (the axial distance between points where the intensity falls to a defined proportion of the peak intensity

$FWHM$ In a distribution of intensity, e.g. at the focus of a lens, the distance between points where the intensity is half that of the peak intensity.

80% LIMIT In a distribution of intensity, the distance between points where the intensity is 80% of the peak intensity.

Resolution in a conventional microscope

For a conventional microscope, the full width 80% LIMIT in the **axial** direction within the image of a point object (i.e. the depth of field FW) is given by

$$FW = 0.51 \frac{\lambda}{n - \sqrt{n^2 - NA^2}} \qquad (1)$$

which reduces to

$$FW \approx \frac{\lambda n}{NA^2} \quad (2)$$

for the case of low (<0.5) numerical aperture.

The FWHM depth is

$$FWHM = 0.88 \frac{\lambda}{n - \sqrt{n^2 - NA^2}} \quad (3)$$

which reduces to

$$FWHM = 1.77 \frac{n\lambda}{NA^2} \quad (4)$$

for low (<0.5) numerical aperture.

In the lateral direction, the resolution, in the FWHM half-intensity sense, is

$$FWHM_{lateral} = \frac{0.51\lambda}{NA} \quad (5)$$

This may be compared with the familiar Rayleigh / Abbe formula,

$$r = \frac{0.61\lambda}{NA} \quad (6)$$

where r is the distance between the intensity peak and the first zero.

In the equations above for a conventional wide-field microscope, the λ is that for the emission wavelength in the case of a fluorescent point object. In a non-confocal flying spot microscope, it is that of the illumination wavelength, which is invariably shorter, so the flying spot has a superior resolution to a conventional wide-field microscope.

Resolution in an ideal Confocal Microscope

By this is meant a confocal microscope with an infinitely small pinhole. The resolution in a confocal microscope comes partly from the illumination, as in other flying spot microscopes, and partly from the effect of the pinhole. It is useful to think of the illumination and detection processes as governed by probability distributions. If the optical system is ideal and the beam filling the back pupil of the objective is uniform in intensity, the intensity profile of the illumination spot will be as in Figure 4 (i.e. it will be the intensity profile of a Airy pattern (Born and Wolf, 1980, p396). This may be considered as the probability distribution for arrival of a photon at any point across a median transect of the illumination spot in a suitably short interval of time. This profile is determined by diffraction within the aperture of the lens. However, if the pinhole is infinitely small, the probability curve for passage of an emitted photon through the pinhole is identical to the

illumination curve. A photon emitted from one of the minima of the illumination curve therefore has minimal chance of detection. The probability of both illumination and detection at a given point in the plane of focus is the product of the two probabilities.

Figure 4 shows how this product, which represents the instrument response curve has a smaller width at half-maximum height than the illumination curve if we ignore the wavelength shift between excitation and emission. The curves drawn in Figure 4 represent Airy patterns, and probably correspond accurately to the distributions in practical confocal systems where the aperture of the objective is well filled. In the case where a Gaussian beam focus is formed and (though rather unlikely) there is a Gaussian detection function, the gain in FWHM resolution is precisely 1.414 (the square root of two).

If we consider again the image of a single point we may describe the axial resolution in the ideal case (with an infinitely small pinhole) as

$$FWHM = \frac{0.64\lambda}{n - \sqrt{n^2 - NA^2}} \tag{7}$$

which, at NA < 0.5 can be simplified to

$$FWHM = \frac{1.28n\lambda}{NA^2} \tag{8}$$

and the lateral resolution is given by

$$FWHM = \frac{0.37\lambda}{NA} \tag{9}$$

The numbers in these formulae, 0.64, 1.28 and 0.37, apply to fluorescent point objects and the wavelength is the geometric mean of the excitation and emission

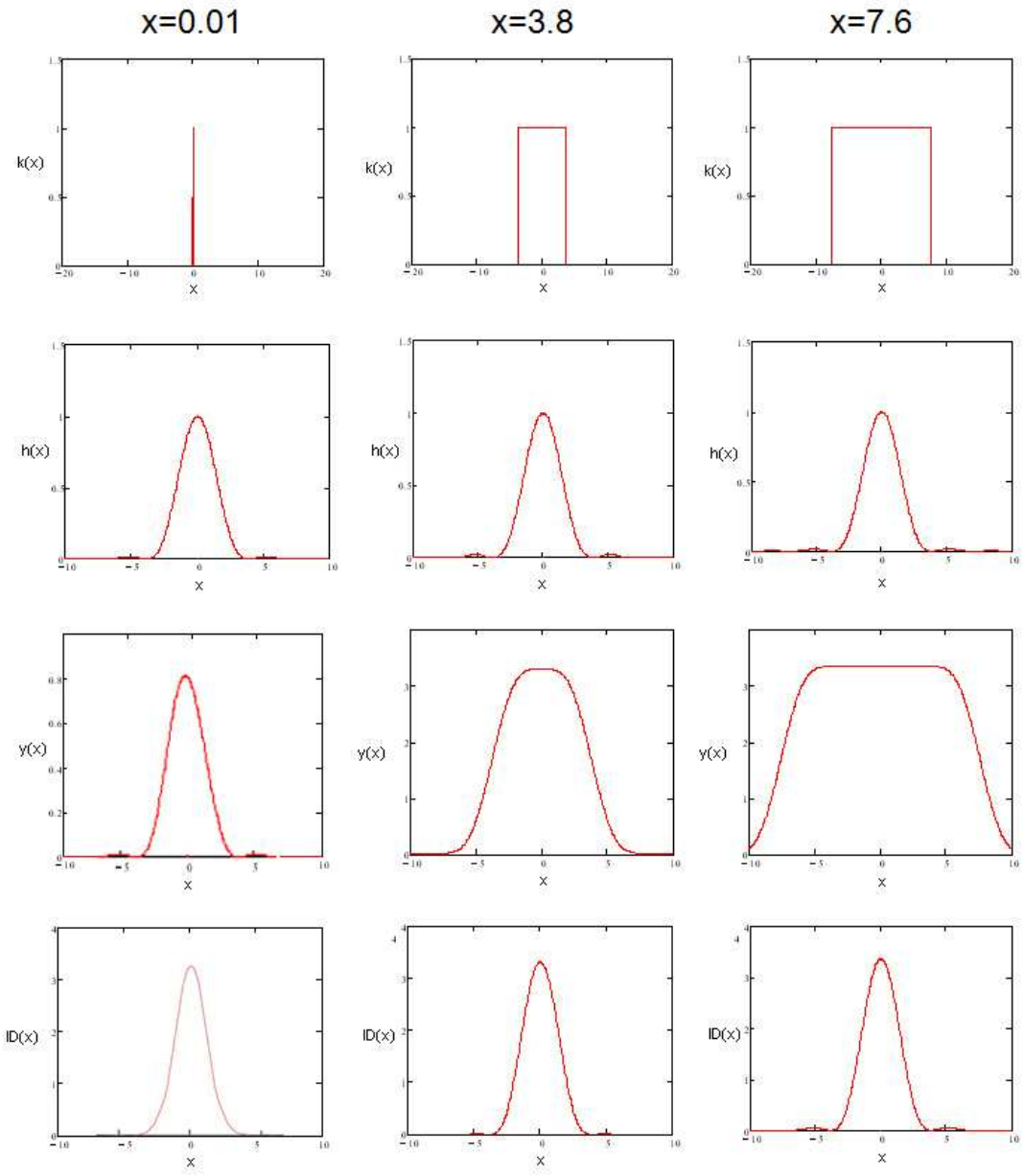

Figure 4

Calculated transverse profiles in a confocal microscope. The top row shows the pinhole transmittance plotted against distance in the plane of focus and the bottom row the instrument response curve. Note that only with a pinhole diameter of much less than one

Airy unit is there an improvement in lateral resolution, shown by the slight thinning of the peak at bottom left and the loss of the subsidiary maxima, which are just visible with the larger pinhole sizes. The illumination function (second row) was calculated as $[(2J_1(x))/x]^2$, where J_1 is a first order Bessel function (Born & Wolf, p396, section 8.5.2). The first minima of this function, which correspond to the dark ring in the Airy pattern occur at x = + and - 3.83. The second row represents the illumination intensity, which is the same for all columns. The third row shows the detectability function, which is the convolution of the pinhole function (top row) with the

illumination function. The bottom row is the result of multiplying the detectability function by the illumination function and represents the instrument response. All curves have been normalised to emphasise the small change in shape on bottom left. Note that this improvement in resolution can be achieved only by a very large loss of signal caused by the nearly-complete closure of the pinhole. Note also that if the pinhole is opened by more than one Airy diameter, there is negligible loss of lateral resolution: the chief loss is of axial resolution, not shown in this diagram.

wavelengths. If we elect to measure the axial resolution of the instrument by considering a thin fluorescent sheet the axial FWHM is given by

$$FWHM = 0.67\frac{\lambda}{n - \sqrt{n^2 - NA^2}} \qquad (10)$$

which is remarkably similar to the expression for a single point. The two responses are not the same since a sheet can be thought of as the superposition of many closely spaced point objects. Naturally the lateral resolution cannot be measured with such a specimen. The $FWHM$ according to this equation are shown in Fig.5 below for the case of air, water and oil immersion.

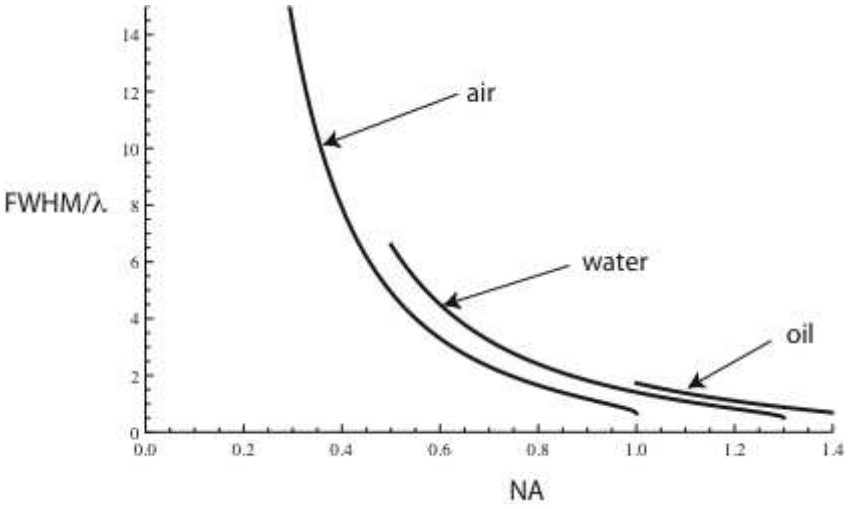

Figure 5. Optical section thickness to the half-peak points in microns divided by wavelength in microns is plotted on the ordinate, with objective NA on the abscissa.

The modest increase in lateral resolution described in Figure 4 for point objects imaged in a confocal microscope, which can be achieved only under ideal conditions, would not justify the use of these microscopes. However, when a three-dimensional object is examined, a striking and immensely useful difference between confocal and both bright-field and flying spot microscopes becomes apparent: the ability to create optical sections. This is the raison d'etre of the confocal microscope.

If, for example, the specimen is a reflective mirror surface in the form of a planar lamina perpendicular to the optical axis, and is perfectly uniform, lacking all blemishes and

dust, its axial position cannot be determined at all with the normal epireflection microscope widefield or flying spot: there is no change in intensity with variation in focus and the height of the surface cannot be determined even by deconvolution of an image stack. But the same specimen, viewed in a confocal reflection microscope, shows a bright image only when the reflecting plane is precisely in focus, and is dark at focal positions above and below that (Figure 6).

This property of 'optical sectioning' can be tested and measured by stepping the focus and taking a series of intensity measurements with such a planar mirror specimen. Juskaitis & Wilson (1999) has developed a real-time focus- oscillating system which displays the position and the apparent thickness of the in-focus layer for demonstration and use by instrument designers. Anyone who has a confocal system can measure the optical section thickness merely by imaging a slightly tilted planar first-surface mirror (Figure 6). The in-focus region appears as a bright band, which in Figure 6 was arranged to run vertically.

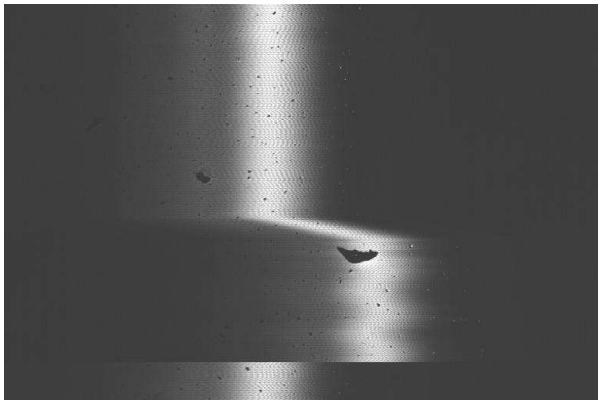

Figure 6 Tilted mirror test for optical sectioning in confocal reflection mode. If a known vertical shift of focus can be imposed (5 μ m in this case) the mirror gradient along a horizontal line in the figure can be deduced.

Axial resolution in a non-ideal confocal microscope (i.e. one in which the detector aperture is not infinitely small)

We could discuss the axial resolution in terms of the image a point object with varying pinhole size and the reader interested in this approach is referred to the detailed discussion contained in the appendix. However, it is perhaps more instructive in this context to consider the image of a thin fluorescent sheet. The image is, of course, featureless but becomes increasingly dim as the sheet is moved away from focus. The rate at which the image intensity decays with defocus may be used as a measure of the thickness of the optical section that the instrument can record. We note that the thickness will be a minimum in the ideal confocal instrument with infinitely small pinhole and become progressively wider as the pinhole becomes increasingly larger. Indeed in the case of the conventional microscope – infinitely large pinhole -- the image signal from a thin lamina sheet is constant and independent of defocus. Wilson [1989] has considered this problem in

detail and has found, see appendix, that a reasonable model to the $FWHM$ of the optical section thickness for practical pinhole sizes is given by

$$FWHM = \frac{0.67\lambda}{n - \sqrt{n^2 - NA^2}} \sqrt{1 + AU^2} \qquad (12)$$

where the pinhole size, AU, is now measured in Airy units. The origin of this equation is discussed in more detail in the appendix and we show below the sectioning strength which may be expected, when using a number of air, water and oil immersion objectives.

.

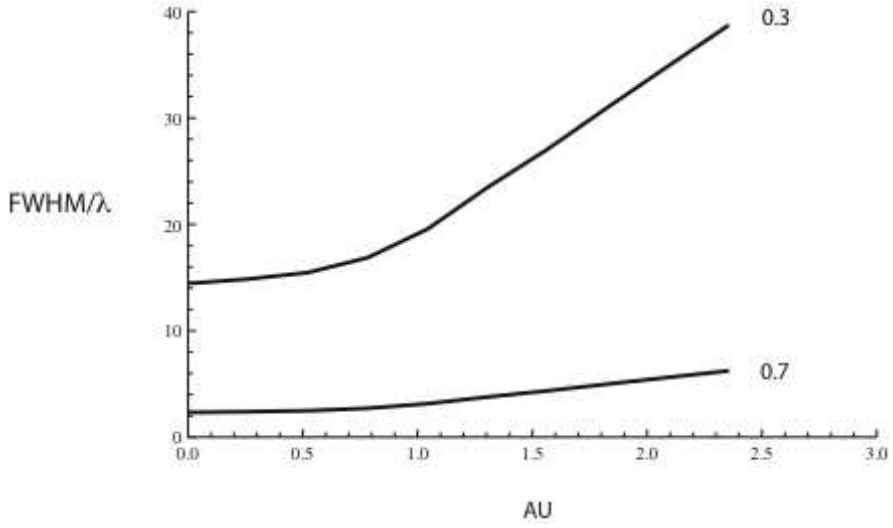

Fig. 7. Half-peak optical section thickness plotted on a vertical scale in microns/ wavelength against aperture diameter in Airy units. The curves are plotted for two dry objectives of numerocal aperture 0.3 and 0.7. To obtain the optical section thickness in microns it is necessary to multiply the value shown on the vertical axis by the wavelength (i.e. for a wavelength of 0.5 um the numerical value has to be halved.

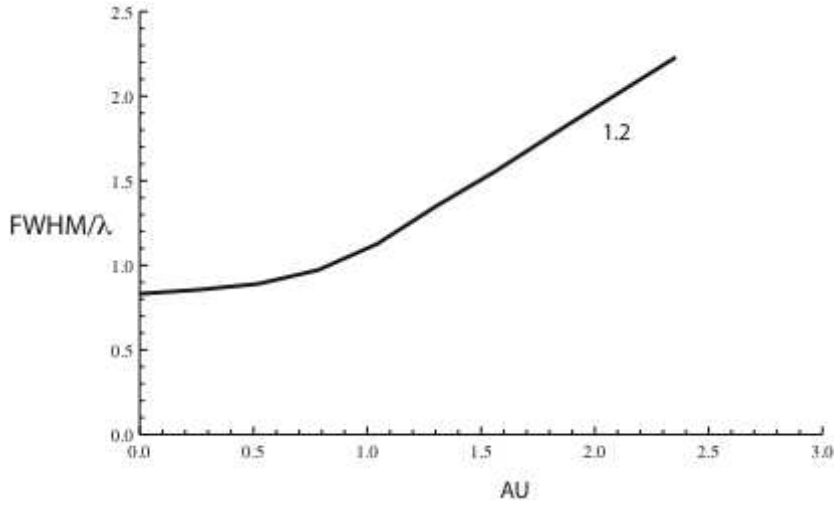

Fig. 8. Half-peak optical section thickness plotted on a vertical scale against aperture diameter in Airy units. The curve is poltted for a 1.2 numerical aperture qwater immersion objective. Vertical axis as for Figure 7

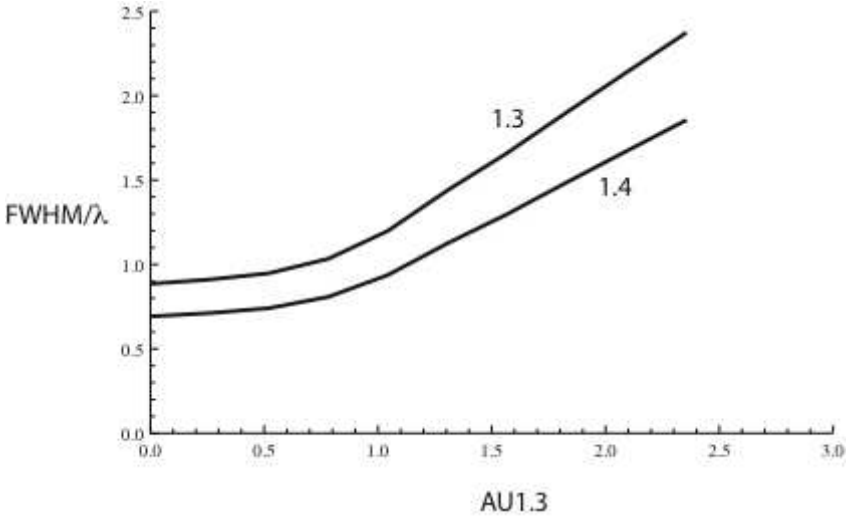

Fig. 9. Half-peak optical section thickness plotted on a vertical scale in microns against aperture diameter in Airy units. The curves are plotted for two oil immersion objectives of numerical aperture 1.3 and 1.4. Vertical axis as for Figures 6 and 7.

Photon Statistics

Most confocal microscopes are used to image the fluorescence of organic dyes or natural biomolecules. The number of photons that can be released from a fluorophore is finite, because all fluorophores are subject to destruction by free radicals, which are generated by side-reactions that accompany the cyclical absorption and emission of photons. If we suppose that the instrument response of a confocal microscope is an Airy pattern, we can ask how many photons are needed to record the profile and begin to see resolution of an emitting centre such as a single molecule.

Four measures will aid this visualization. One is to increase the magnification until only three pixels span the Rayleigh resolution distance (i.e. half of the diameter of the Airy disk to the first dark ring). This, which can be achieved by reducing the scale of the scanned raster while keeping the dwell time per pixel constant, will give the maximum numbers of photons per pixel while still offering the chance of resolving the Airy pattern. It is a practical application of the Nyquist rule in information theory, that the sampling frequency must be twice the highest frequency to be found in a signal, if no information is to be lost. The second is to remove all external sources of photons and the third to immobilize the source molecule: Brownian motion will otherwise smear out the pattern and prevent resolution. Fourthly, it will be advantageous when there is any movement that cannot be eliminated to use a fast scan with few scan lines: a confocal microscope normally visits each spot only once, for a few microseconds, in a 500 line scan, which may take a full second to complete: the effect of slow movement can be mitigated by using a faster framing rate.

A computer simulation (Fig 10) shows the images of three molecules each formed by the same number of photons in a Poisson distribution conditioned by an Airy-type instrument response profile. Two molecules are placed at the Rayleigh resolution distance apart: the third is more distant. It can be seen that although only a few tens of photons are necessary for detection, at least 500 photons are required to resolve the close pair according to the Rayleigh criterion of seeing a dip in intensity between them, even under these ideal conditions. To give the highest possible photon count in each pixel, the pixel size is set as large as possible without exceeding the Nyquist limit (i.e. the diagonal pixel spacing is ¼ of an Airy Unit.

This simulation highlights the serious problem of noise in fluorescence imaging. A typical fluorophore may survive only long enough to emit 30,000-40,000 photons (Tsien & Waggoner 1995) . Most of these will be emitted in the wrong direction and not pass into the objective, and a further reduction to only a few percent is likely to occur in the optics of the microscope. Moreover the shot noise modelled here is not the only source of noise in the imaging process and the model has no background noise. It is doubtful whether a single molecule will ever be *resolved* as an Airy pattern of high quality in a confocal microscope, though the *detection* of such molecules in wide-field microscopes is now routine.

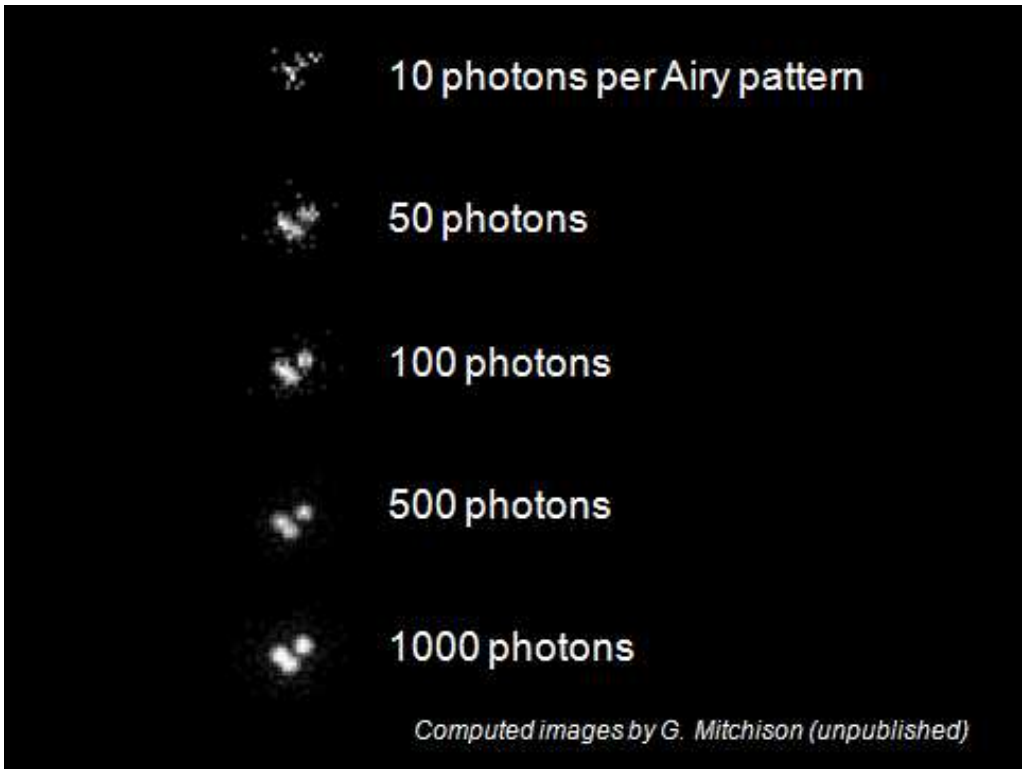

Figure 10 Computer simulation of the imaging of three emitting points (e.g. three fluorophores) at the minimum magnification, below which spatial information would be lost. Note that a large number of photons must be detected at each point in order to have resolution of the two closer points, which are set at the Rayleigh resolution distance apart.

Parallel confocal microscopes: scanning slit and spinning disk systems

In one sense, the single-point scanning confocal microscope has very great time resolution. It can be set to scan on a line, and in a modern fast resonant system, the line rate is 15 KHz, so an object in the centre of the scanned 15 times per millisecond: faster than any biological event. But when it is producing high-resolution frames, it is very slow, typically one frame per second at 500 x 500 pixels. There is also a long lag between the collection of data from objects at the top of the image and the bottom, so that synchronised events such as may occur in a field of neurones cannot be recorded over the whole area. There is a need for a faster confocal system than the single point.

Petran developed in 1965 a massively parallel system, based on a spinning disk perforated by thousands of tiny holes, which was made by hand by his colleague Hadravsky in Prague (Petran et al. 1985). This has been described as a Nipkow disk, but the latter was designed to bring into the field only one spot of light at a time: Petran's disk had thousands of holes, each generating a spot of light on the specimen, which was then imaged through

a particular hole in a symmetrical array of holes on the opposite side of the disk. This was, in effect, thousands of confocal optical systems acting in parallel, and when the disk was spun at sufficient speed, a continuous confocal image could be viewed by eye or photographed. The original Petran microscope had a system of prisms to bring the returned images of the holes into the correct orientation and suffered from low transmission, of the order of 1%, which made it useless for low-light-level fluorescence work. A great improvement was made in the Yokogawa Electric Company (Japan) by introducing a second disk, coaxial with the perforated disk, and carrying an array of microlenses of long focal length (Tanaami et al. 2002). The lens disk was mounted rigidly on the same axle as the perforated disk (see figure 11), so that they rotated in precise synchrony as one unit .

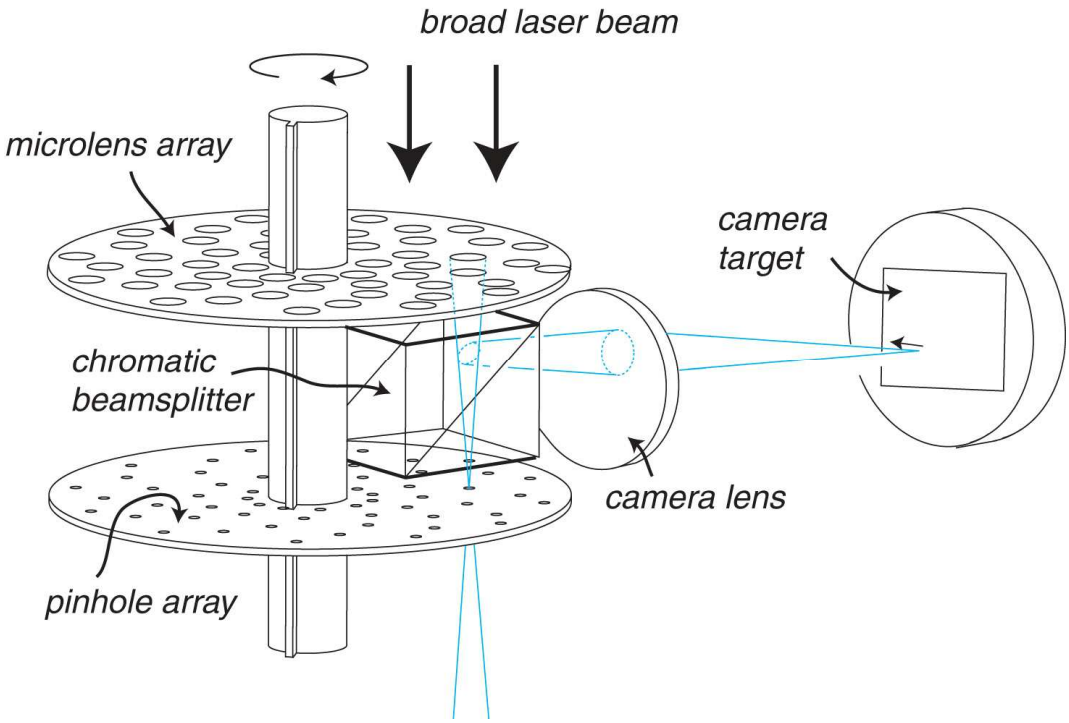

Figure 11. Spinning disk system showing the double disk introduced by the Yokogawa Company, with a lens disk rotating in synchrony with the perforated disk.

The microlenses were used to concentrate the light into the pinholes in the disk, thus solving the two problems that had bedevilled previous designs: the transmission was increased to as high as 40% and the back-scatter from the perforated disk was also greatly

reduced. A chromatic reflector directed the emitted light selectively to a camera because of its longer wavelength. Laser light was also used in preference to the arc lamps used previously, because high collimation was needed for the microlenses to work properly. The Yokogawa design has now been taken up by several manufacturers and is widely used, particularly in electrophysiology, where large fields must be studied with high time resolution. Coupled with modern electron-multiplier charge coupled device cameras (EMCCDDs), the spinning disk confocal systems have now become the system of choice for following rapid particle movement in cells as well as calcium sparks and other transitory events, where framing rates of 100 per second or more can be used.

Another method for introducing parallelism is to scan a bar of light over the specimen, and to have a slit as the confocal aperture. This also allows very rapid framing. Commercial systems based on the designs of Brakenhoff and of White et al. (see Amos and White, 1995)have been produced. These systems were developed with the idea that a stationary slit aperture could be varied in width (unlike the holes in the spinning disk), for the same purpose as the variable aperture in the point scanning systems (i.e. to strike an appropriate compromise between ideal confocal performance and signal strength). The slit-based systems have not found much favour, possibly because the illumination intensity conforms to a $1/d$ rule rather than $1/d^2$, where d is the distance from the focal plane) and the optical sectioning effect is in practice intermediate between a point-scanning confocal system with a small aperture and a conventional wide-field system.

The 'swept field' system of Prairie Technologies (USA) is unique in being variable between a slit confocal scanner and a multi-point scanner, in which the points are few and widely-separated, so that 7 horizontal swathes of the image are scanned simultaneously. With the 7-point scanner, the confocal performance is similar to a single-point scanner, and different aperture sizes can be selected, while the slit can be selected instantly for ultra-fast imaging.

Direct View

Originally, the visible optical image was seen as a great advantage of the parallel confocal systems. Except in the Zeiss 5-Live system, efforts were made to provide at least one eyepiece, through which the confocal image could be viewed. In the slit-scanning system of White et al. a second scanning system was used to cause the image to oscillate in a direction perpendicular to the length of the slit, thus presenting a 2-dimensional image to the eye. Brakenhoff's design was more elegant, using the rear surface of the scanning and descanning mirror to rescan the post-aperture image. These systems provided a good demonstration of the fact that useful improvements could be gained even when the aperture was far from the confocal ideal size. Unfortunately, when fluorescent specimens were viewed by eye in either the slit scanning or Yokogawa spinning-disk systems, a high rate of bleaching was observed. The eyepiece on modern Yokogawa systems is now often inconveniently placed and seldom used, presumably for this reason.

Comparing spinning disk and single point confocal systems

Few subjects in the confocal sphere have caused more controversy than this, fuelled by commercial interests as well as competition between experts. Before attempting a discussion of this comparison, it is worth pointing out that some of the advantages of a flying-spot system are lost as soon as one departs from a single scanning spot. The most obvious is the automatic register of multiple channels: multiple cameras or some equivalent system whereby separate recordings can be made and brought into spatial and temporal register are needed. Secondly, the capacity to zoom the image while keeping the same number of pixels is lost, and thirdly the ability to adjust the pinhole size is lost in the spinning disk case and the size may not be correct for more than one type of objective lens.

Before any comparison can be made, several points must be checked in both the single-point and the spinning disk system. Most published comparisons are invalid because one or more of these points has not been considered.

1. The specimen, the focal level in the specimen and the magnification and area covered must be the same.

2. The wavelengths used for excitation and emission detection must be the same.

3. The objective lens and its numerical aperture must be the same.

4. The image quality must be assessed by an objective criterion, such as a numerical measurement of signal-to-noise ratio, as advocated by Murray (1998).

5. The radiation damage to the specimen must be measured since this is the only reliable indication of the amount of energy absorbed by the specimen during the imaging process. The amount of bleaching per frame is a convenient measure for this quantity.

6. The degree of confocal stringency must be the same. This means that the aperture size, back- projected into specimen space and the confocal section thickness must be the same.

The most careful comparison, in which efforts were made to control all of these points, is that of Wang et al. (2005) who compared various point-scanning confocal systems with a Perkin Elmer Ultraview Yokogawa system equipped with a Hamamatsu Orca-ER CCD system.

When fluorescent beads of 2.5 μm diameter were imaged at the same bleach rate, other conditions being kept the same as far as possible, the signal-to-noise ratio in the Yokogawa system was at least four times higher than with the single point system. (No details are given of which single-point system was used in each experiment, nor of whether the single point systems varied). When conditions were adjusted to produce single frame images that were comparable in quality, the photobleaching over subsequent frames was found to be 15 times faster in a single-point system than in the Yokogawa.

The weakest point in this comparison is in point 6. Here the manufacturer's data was accepted that the diameter of the holes in the Yokogawa system was the equivalent of

one Airy disk, when the recommended 100x objective of NA 1.4 was used, and the single point system was set at 'one Airy disk', using the software provided. According to Toomre and Pawley (2006) the Yokogawa aperture size is 50 μm, but the FWHM spot size for green light of 543 nm wavelength, given by equation (5) is 19.8 um, so the diameter of the Yokogawa pinhole is actually equivalent to 2.5 Airy Units in this sense. Also, the manufacturers of single point systems do not publish their actual pinhole sizes and different equations seem to be used to calculate their Airy calibrations, which might well be in error.

To check this independently, Wang et al. tried to measure the axial resolution with subresolution (100nm) beads. The axial FWHM measurements were 0.71 μm for the Yokogawa, compared with 0.6 μm for the single-point system. However, the bead is a poor test object for measuring confocal stringency: the equation for non-confocal axial $FWHM$ derived here (equation 1, above) suggests that a wide-field microscope with no confocal optical sectioning whatever (i.e. no pinhole) would have an axial resolution of 0.47 μm (assuming n= 1.515 ,NA 1.4 and λ = 0.543). It is, in fact, very difficult to measure the axial resolution of a Yokogawa system: the step-function specimen (see next section) normally gives a much inferior depth resolution to a point system, but this is usually explained as due to cross-talk between the holes.

Wang et al. commented correctly that the relatively large improvement in signal-to-noise could not be explained by the improved quantum efficiency of the CCD detector compared with the photomultiplier (which is usually adduced to explain such results) and were at a loss to explain it at all, since a 16-fold improvement in signal (integrated over the period of collection of one frame) would be needed to produce a four-fold S/N improvement. This has been observed repeatedly and no convincing explanation has been put forward for it. The most likely explanation seems to be that the confocal stringency of the Yokogawa system is much less than is assumed, so that the illuminated and photometric volume is increased (mainly by an axial stretching): a 2.5-fold increase in pinhole diameter relative to that used in the point scanners could give rise, by assuming a cubic increase, to a volume increase of 15.6 times in the illuminated and detected volumes, which would allow much lower laser intensities to be used, because more fluorophores would be present in the enlarged volume. The cubic approximation may not be unreasonable, since an increase in the size of the pinhole in a spinning-disk system increases the illuminated volume as well as the photometric volume, so its effect on signal strength would be greater than the effect of opening the detector pinhole in a single spot scanning system.

It is observed that when the detection aperture of a single point system is widened, signal increases of this order can be obtained and laser powers can then be reduced with concomitant reductions in photobleaching. In order to exploit this effect, an inverted telescope was devised and produced for the Bio-Rad Radiance single-point systems, which allowed the equivalent of a very large pinhole to be used. This gave results very similar to the Yokogawa system, with good lateral resolution (as expected), poorer axial resolution,

very low photobleaching rates and greater longevity of living specimens (Reichelt & Amos, 2001) .

The measurements of Wang et al are exceptional in their attempt to control all the necessary parameters, but clearly, even more needs to be done before the functioning of these different systems can be compared and understood. Meanwhile, the spinning disk systems are the only ones that can image fast events in large fields such as 1000 x 1000 pixels with any degree of optical sectioning ability : they are undoubtedly useful, and further experiments are needed to find out why they are so good.

Testing a confocal microscope

Confocal systems are complex and tend to be used communally. It is useful to have standard test procedures for checking the condition of systems as well as comparing them.

General Testing of Environmental Effects

Oscillations are often seen in confocal systems. It is important to establish whether these are electronic or mechanical in origin. **Vibration** effects are almost always due to relative movement of the objective and specimen, and tend to be more prominent at higher magnifications. Any specimen with a vertical edge or scratch (including the paper slides described below) will show a wavy profile if the stage of the microscope is vibrating in the horizontal direction with respect to the image. Interferometry makes it possible to measure vibrations precisely. An apparatus which is easy to construct (FIg 12) makes it possible to obtain multiple beam fringes, according to the Tolansky method (Tolansky ,1970) . These sharp fringes occur when an in-focus plate is brought within a few wavelengths of a reflecting surface on a microscope stage. If a confocal system is set up with a monochromatic laser beam and fringes are produced which lie vertically in the image, axial vibrations of the objective relative to the stage cause horizontal deviations of the fringes, as shown in Fig 12 . All microscopes tested , even those securely bolted to a massive anti-vibration table, tend to show movements of approximately 200nm at audio frequencies of a few hundred Hertz. These are worsened if an air-conditioning plenum or fan is situated nearby. The visible oscillations should not be confused with the regular mismatch of alternate scan lines which occurs because of a lack of registration between successive scans, which is often seen in bidirectional scanning systems. Microphonic effects on single mode fibres have been mentioned above (under ‘Beam Scanning Microscopes’).

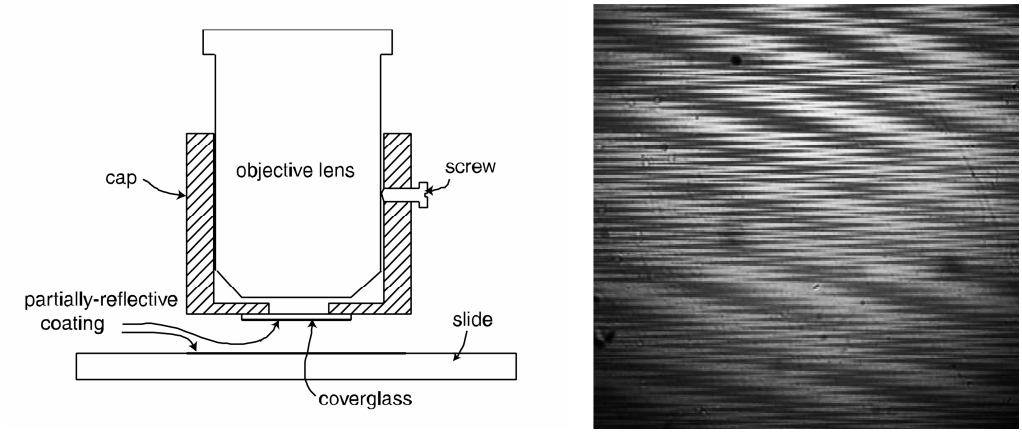

Figure 12. A simple but quantitative vibrometer for recording axial vibration of the objective relative to the slide. A cap is fitted over a low-power objective, e.g. a 10x dry, and adjusted in position until a reflective aluminium or silver film on the undersurface of a coverslip attached to the cap is in sharp focus. When the assembly is brought within a few wavelengths of a reflective coating on a slide, multiple beam fringes appear (Tolansky 1970) which can be arranged to lie approximately vertically in the image by small tilt adjustements of the slide. As shown on the right (a scanned transmission image shows fringe deviations of more than two hundred nm (the fringe separation is equivalent to one half wavelength in height change) occurring at a few hundred Hz , due to resonances in the body of the microscope generated by ambient sound. For reflection imaging, a fully reflective mirror can be used on the slide rather than a semi-transparent one. Tolansky recommends the use of silver instead of aluminium, or a rutile plate instead of a vulnerable exposed metallic coating. If the upper and lower reflecting surfaces are brought into contact the fringes become straight.

Temperature may also affect performance. Apart from direct effects on certain lasers, the ambient temperature may affect the amplitude of scan of the scanning mirrors. This is best tested by the use of silicon test targets marked with squares with precise position and spacing (available from electron microscopy suppliers). Unless there is precise indexing of movement by an encoder, the magnification may show warmup variation of 10% or even more. If magnification is critical, internal length standards such as spherical beads should be included with the specimen.

Test Slides

These are indispensible and need to be easily and cheaply made, since they are always lost or destroyed in systems used communally, often by being left soaking in immersion fluid. The following have been found to be generally useful in biomedical labs. For all of these specimens, circular coverslips with a diameter of 22 mm and a thickness of 0.17 mm are best, since square coverslips cannot be ringed to protect the preparation. The technique of ringing by means of a turntable and paintbrush loaded with varnish is described in old manuals of microscopy. Modern immersion fluids attack most types of varnish, but 50% fresh shellac dissolved in methanol proves to be resistant.

1. A planar reflector.

This is used (as described above and in Fig 6) to check axial resolution and to examine the kinetics and repeatability of the motorised focus. It also reveals any departure from flatness of field, and shows up any falloff of image brightness towards the edges of the scan, which is an indication of incorrect scan geometry. A simple front-surface mirror is not suitable for work at high numerical aperture, since the objective is designed to be used with a coverglass. Aluminium can be deposited on one surface of a clean coverslip , using a standard evaporator (used for electron microscopy) with a tungsten filament as the source of heat for melting a small fragment of aluminium foil. The coverslip can then be mounted, aluminium coated surface facing downwards, on a standard microscope slide and fixed in position with a setting mountant or an ultra-violet –cured glass cement. Tiny holes and scratches in the aluminium can be made by dabbing the exposed surface with a stiff but fine paintbrush. This allows the focus in reflection to be checked (it may not correspond to the brightest image) and makes the same specimen useful in transmission for testing for chromatic aberration.

2. A step-function fluorescent object.

This type of specimen, advocated by Stelzer and Wijnaendts-van-Raesandt (1990) as a general test for confocal performance, is useful for measuring axial resolution in fluorescence at different detector aperture settings. The specimen presents a boundary between a homogeneous fluorescent medium and a non-fluorescent coverslip. We have devised a cheap and convenient form, consisting of a permanent resin which is a refractive-index match for the coverslip glass (Histomount : Fisher Scientific) in which 5 ug/ ml of the red dye Nile Red (BDH Gurr ?) or the fluorescein-like laser dye Coumarin 6 (Eastman Kodak Co) is dissolved. A z series of images (or xz scan, if the system is capable of this type of scanning) shows, ideally a vertical step from zero signal in the coverslip to a high fluorescence emission in the dye solution. In reality, a sigmoid curve is obtained, and the axial distance between the 20% and 80% points on the curve form a useful indication of confocal stringency. A conventional microscope gives a high intensity at all levels, i.e. a flat plot with no step.

3. Standard fluorescent specimens

Many biological experiments are conducted with material that is difficult to obtain and which shows capricious staining and sometimes none and deteriorates rapidly. It is useful to have ready to hand fluorescent specimens that are permanent.

Confocal systems are normally supplied with commercially-prepared test specimen such as botanical sections stained with unknown dyes and mounted in unknown media. The following specimens have been found useful and easy to prepare with the usual facilities of a biological lab.

3a. Fluorescently-stained paper. Paper stained with safranin (Fisher Scientific) is brilliantly fluorescent with green excitation and shows acceptable signal at all excitation wavelengths that are used in confocal work. This dye is soluble in water but not in xylene

and the stain is fast in paper mounted in Histomount or similar non-fluorescent resin dissolved in xylene .

10mm squares of thin paper (e.g. air mail grade) are stained in a 0.1 % solution of safranin in water for 30 min or longer, with a magnetic stirrer, and the paper is then dehydrated in ethanol and cleared in xylene (as is usual in histological slide preparation). The paper is then soaked in HIstomount made mobile, if necessary, by the addition of xylene and then each square is mounted under a circular coverslip under slight compression with a small weight or slide clip to hold the paper flat. After leaving overnight on a hotplate the slides are ringed .

3b. Fluorescently-stained *Daphnia* . The cladoceran ('water flea') *Daphnia* is readily obtained from freshwater ponds and lakes or can be bought from aquarium suppliers. Each organism is a few millimetres in diameter and contains much intricate structure which is ideal for teaching and demonstrating three-dimensional imaging in confocal microscopy.

The organisms can be killed and fixed in 70% ethanol and stored in ethanol for weeks before staining. Spirit-soluble eosin in ethanol is used and the specimens are then dehydrated rapidly in ethanol , cleared in xylene and soaked in Histomount, preferably overnight, before mounting. Since the organisms are quite large and brittle once dehydrated, it is best to mount them in single-cavity slides, allowing xylene to evaporate before covering them with a thin layer of Histomount and adding a coverslip. The coverslip may be prevented from lying flat by the specimen: this can be cured by placing a small weight such as a steel nut on top of the coverslip.

3c. Autofluorescent pollen grains.

This specimen is highly bleach-resistant and useful for testing objectives of high NA. , particularly the *Spathiphyllum* pollen, which has very closely-spaced fluorescent lines. Pollen grains have in their hard external cell walls an autofluorescence, possibly due to stable carotenoid pigments, which persists even in fossil material. To collect pollen, remove the stamens of suitable plants such as *Passiflora, Taraxacum, Cobaea, Lilium or Spathiphyllum* and store them in glacial acetic acid. Subsequent processing requires a fume cupboard and safety precautions. Rinse in fresh acetic acid, centrifuge down and transfer to concentrated hydrochloric acid. Heat in the concentrated acid and replace this with concentrated sulphuric and nitric acids to oxidise most of the organic material and finally heat in acetic anhydride before transferring to water. Dehydrate in ethanols, clear in xylene and mount in Histomount. The autofluorescence is best excited with green light: there is a strong emission in the red.

3d. Fluorescent beads.

Fluorescent beads, usually of polystyrene containing proprietary stains, are universally used for testing microscopes. The mounting method is critical to their successful use. The beads must be immobile, for Brownian motion in a fluid, even a viscous one like glycerol, makes accurate imaging impossible. It is best if the beads all lie in a single

plane. They must not, however, be dried, because they shrink and the imaging conditions will be highly abnormal if they are surrounded by air. The method we have used is to clean the coverslips with an abrasive domestic cream cleaner and then deposit a very dilute suspension of beads in distilled water in a drop covering much of the surface, which is then allowed to evaporate overnight at room temperature. The beads become firmly attached to the glass and remain attached when the coverslip is inverted over a drop of gelvatol medium on a glass slide. Gelvatol is a solution of polyvinyl alcohol in water which sets hard when water evaporates from it. It is better to use a known mixture than to use one of the many proprietary mountants. The following formula can be use for biological specimens, including immunofluorescent preparations , as well as beads.

Add 21g of polyvinyl alcohol (SIgma P-8136) to 42ml glycerol. Add 52ml water with a crystal of sodium azide as preservative and 106 ml Tris buffer, 0.2M, at pH 8.5. Stir , warming gently if necessary, until dissolved. Centrifuge at 5000g for 15 minutes to remove undissolved material, distribute aliquots into Eppendorff tubes and store at 4 degrees C. It is best to an an antifade compound: diazo-bis-cyclo-actane (DABCO) at 2% w/v results in slower setting but prolongs fluorescence.

Future developments.

Since its widespread introduction in the 1980s, the laser scanning confocal microscope has become standard equipment in almost all laboratories in the biomedical field, and has even been used in geology and materials sciences, including research in foodstuffs and cosmetics. It has furthered the trend for end-users (i.e. researchers) themselves to seek improvements in microscope technology and this trend, which is altering the nature of the microscope industry, is likely to continue.

Low fluorescence signals mean that improvements in detector technology are constantly sought. Hybrid detectors, such as those which are half-photomultiplier and half-avalanche photodiode have already proven popular, with a gallium arsenide phosphide (GaAsP) photocathode improving the sensitivity over a wide dynamic range. Since more than one detector is usually needed in a microscope system, opportunities exist for alternative semiconductor materials, such as GaAs and GaP, which may have increased quantum efficiency over a more narrow spectral range.

As well as the efficiency limitation, detection speed is also a key issue. In recent years, single-photon avalanche detectors have proved able to detect very low intensity signals (down to the single photon). Moreover, these devices have very high temporal resolution (few tens of picoseconds) and a fast response time, and thus are particularly useful in lifetime measurements and applications where a fast signal is to be detected, e.g. in confocal fluorescence correlation spectroscopy and confocal ratiometric imaging. Within the field of confocal, these devices are just beginning to show their potential.

The excitation source is also undergoing continual development. The use of a gallium nitride laser diode in confocal microscopy proved that cumbersome gas lasers, which generate unwanted heat and vibration as well as emission intensity noise were no

longer required and this set the benchmark for the laser developers. The most suitable solid-state lasers for confocal imaging are infrared emitting diode or vertical external-cavity surface-emitting laser (VECSEL) devices, frequency doubled, tripled or Raman shifted to reach the desired wavelength. At present, the VECSEL systems tend to be optically pumped, but many research groups worldwide are engaged in the development of electrically pumped VECSELs: this advance would render a research grade system fit for integration into commercial systems. VECSELs are compact systems with low noise and can be designed to give a beam quality close to M^2=1. With developments in semiconductor gain materials, particularly in the field of indium gallium nitride (InGaN), which spans the entire visible range, we envisage that new materials will provide greater wavelength flexibility for confocal excitation.

To complement this activity, developments in optical fibre-based laser sources have great potential. We have already seen the application of the white-light supercontinuum source in confocal microscopy, but many other fibre-based systems exist and, with developments in doped fibre systems and photonic crystal fibres, diverse laser platforms are likely to emerge.

However, it is within photochemistry where we see the most significant opportunities. There would have been little incentive to develop the confocal microscope had it not been for the specific fluorescent labelling methods, which began their explosive development in the 1970s and 1980s,and improved fluorochromes and photoprotein methods are now appearing every month. The efficiency of the excitation source and the detector are ultimately limited by weakly emitting fluorophores: typically the researcher bombards the specimen with excitation photons and uses high-gain detection to overcome this problem, but this approach is not particularly kind to the organism under investigation! For practical live cell confocal imaging, even small improvements in photochemistry are likely to have large impact. Label-free imaging is also advancing, but is difficult. For example, confocal Raman is usually not suitable for live cell analysis because of long acquisition times that are incompatible with sample movement and autofluorescence. While useful in some biomedical specimens, it tends to lack chemical specificity.

Another problem with existing confocal microscopes is the breakdown of the confocal optical sectioning at low magnification. This is a consequence of the low numerical aperture of standard microscope objectives of low magnification. For example, a standard 4x objective of high quality may have NA = 0.2. From equation (8) it follows that the axial resolution, even under ideal confocal conditions, is only 16 um. A novel type of 4x objective lens, with a field diameter of 6 mm an NA of 0.46 has been developed by WBA and E. Reid in Cambridge. The lateral resolution of this lens is more than twice that of the standard lens and the axial resolution is 4 um. This unusual lens (50cm long) is now being developed as the basis of a laser scanning confocal microscope in Strathclyde by WBA and GMcC. It has already proved useful as a camera lens for the study of large objects such as whole mouse embryos, showing subcellular detail as well as gross anatomy in the same image (see http://www2.mrc-lmb.cam.ac.uk/va/newgiantlens/.)

A trend towards megalithic systems which cannot be modified or even opened without invalidating warrantees has developed, but this will probably be balanced by the development of kits and shareware designed for the scientist who wishes to build a system to suit a particular requirement rather than rely on a commercial product.

Although confocal microscopes are standard tools in all biomedical research labs, cost has prevented them from being adopted widely in diagnostic medicine. Cost is clearly the issue, since their obvious potential for examination of biopsy material , in which living cells , including details of such cytological features as brush border of kidney tubules, was pointed out early (White and Amos, 1987)and sporadic experiments have been made since (e.g. Ball et al. 1994)). The laser developments mentioned above, together with clear definition of a more limited range of functions, may bring cost down to a tipping point where the confocal microscope becomes universal in diagnosis and then so cheap that individual scientists can easily afford it. Only then will the potential human benefit of this technology be fully realised.

Optical Appendix

1. Optical Units

In this discussion, r denotes distance in the radial direction perpendicular to the optical axis and z represents length along the optical axis, n is the refractive index of the medium, $NA = n\sin\alpha$ where α is the semi-angle of the cone of light forming the focus, i.e. the ray which has the highest angle to the optical axis. The wave-vector k, which equals $2\pi/\lambda$ is a useful conventional quantity to include the effects of wavelength.

The size and shape of the pattern of light at the focus of a perfect lens varies according to the wavelength and numerical aperture. These changes could be shown by plotting the intensity against a radial coordinate r and an axial coordinate z in units of length (e.g. microns) for a specified numerical aperture, wavelength and immersion medium. However, it is convenient to introduce new (optical) coordinates, u and v which are proportional to *r* and z such that

$$v \textbf{ (radial coordinate) } = krn\sin\alpha \qquad \text{(A1)}$$

$$u \textbf{ (axial) } = 4kzn\sin^2\left(\frac{\alpha}{2}\right) \qquad \text{(A2)}$$

u and v are dimensionless, since they each contain one length divided by another length (r/λ and z/λ respectively). (n, being a ratio of speeds, is also dimensionless).

If these coordinates are used the shape and size of the focus is fully defined for all values of wavelength and numerical aperture. As an example the first zero in the intensity

distribution in the focal plane ($u = 0$) occurs when v = 3.83 = 1.22 π. We may convert this back to a real distance, r, using equation (A1) to confirm that the first zero occurs when $r = 0.61\lambda / n\sin(\alpha) = 0.61\lambda / NA$. Further the first zero in the axial direction occurs at $u = \pm 4\pi$. A detailed map of the focal region in u and v coordinates is given, for example, as Figure 8.41 of Born and Wolf.

The use of the 'optical units' u and v is attractive since they allow calculations to be made that are applicable to all foci formed by all perfect lenses. The convenience of doing this, however, is balanced by the need to translate the results back into r and z coordinates, i.e. real lengths, before they can be compared with experimental data.

2. The dimensions of the point spread function in a conventional microscope

In fluorescence, the image formation may be described as

$$I = |h|^2 \otimes f \qquad \text{(A3)}$$

in which I signifies intensity, $h(u,v)$ is the amplitude point spread function of the imaging lens evaluated at the fluorescence emission wavelength and f denotes the distribution of the fluorophore. The symbol $\otimes$ denotes the convolution operation.

As described in Born and Wolf, the structure of the focus of a perfect lens is such that

$$h(0,v) = 2\frac{J_1(v)}{v} \qquad \text{(A4)}$$

where $J_1(.)$ denotes a first order Bessel function of the first kind. Furthermore,

$$h(u,0) = \frac{\sin(u/4)}{u/4} \qquad \text{(A5)}$$

.

and we have ignored phase factors for convenience.

3. Resolution in the conventional microscope

We elect to consider resolution in terms of the image of a single point object. In this case the image maybe written, from equation A3 as

$$I(u,v) = |h(u,v)|^2 \qquad \text{(A6)}$$

We now use this equation to estimate the **axial** resolution by setting $v = 0$. It is now a matter of choice as to how to measure the width of the function $|h(u,0)|^2$. It might be thought that the width of the image between the points where the intensity falls to 80% of the peak was reasonable. In this case we must solve

$$\left(\frac{\sin(u/4)}{u/4}\right)^2 = 0.8 \qquad \text{(A7)}$$

The solution is given by $u = u_{0.8}$ together with $u_{0.8}/4$ = 0.809. The problem is now to find the value of z corresponding to this value of u. Using equation (A2) we may write the full width, FW, as

$$FW = \frac{0.809\,\lambda}{\pi\, n \sin^2\left(\alpha/2\right)} \qquad \text{(A8)}$$

which is rather unwieldy and difficult to relate to the actual numerical aperture. However two simple trigonometric identities can be used to cast this equation into a more manageable form. We first note that

$$\cos(\alpha) = 1 - 2\sin^2\left(\alpha/2\right) \quad \text{and} \quad \cos^2(\alpha) = 1 - \sin^2(\alpha) \qquad \text{(A9)}$$

which permits us to write $2\sin^2\left(\alpha/2\right) = 1 - \sqrt{1-\sin^2(\alpha)}$ and hence

$$n\sin^2\left(\alpha/2\right) = 0.5\left(n - \sqrt{n^2 - n^2\sin^2(\alpha)}\right) = 0.5\left(n - \sqrt{n^2 - NA^2}\right) \qquad \text{(A10)}$$

and finally

$$FW = \frac{0.51\,\lambda}{n - \sqrt{n^2 - NA^2}} \qquad \text{(A11)}$$

We note that if the aperture is small we may approximate

$$n - \sqrt{n^2 - NA^2} = n - n\sqrt{1 - \left(NA/n\right)^2} \approx n - n\left[1 - \frac{1}{2}\left(NA/n\right)^2\right] \approx NA^2/2n \qquad \text{(A12)}$$

and hence

$$FW \approx \frac{\lambda\, n}{NA^2} \qquad \text{(A13)}$$

We have arrived at this result by considering the 80% width of the image. Had we decided that the width of the image between the points where the intensity falls to 50% of the peak was reasonable then the solution would have been given by $u = u_{0.5}$ and $u_{0.5}/4$ = 1.4. In this case the expression for the 'full-width-half-maximum" takes the form

$$FWHM = \frac{0.88\,\lambda}{n - \sqrt{n^2 - NA^2}} \qquad \text{(A14)}$$

which reduces to $FWHM \approx 1.77\frac{\lambda n}{NA^2}$ in the low aperture case.

In order to discuss **lateral** resolution we consider the image of our point object in the focal plane (u *=0*) which is given by

$$I(0,v)=\left(2\frac{J_1(v)}{v}\right)^2 \qquad \text{(A15)}$$

If again we measure resolution in terms of the half width then the value of v at which $I(0,v)=0.5$ is given by v = 1.62. It is straightforward now, using the definition of equation (A1) to write

$$FWHM=\frac{1.62}{\pi}\frac{\lambda}{n\sin(\alpha)}=0.52\frac{\lambda}{n\sin(\alpha)}=\frac{0.51\lambda}{NA} \qquad \text{(A16)}$$

We note, in closing, that had we chosen to measure resolution in terms of the positions of the first zeros, i.e. $I(0,v)=0$, then the solution requires $v=1.22\pi$ which results in the familiar Rayleigh criterion of $FWHM=1.22\lambda/NA$.

4. Resolution in an ideal confocal microscope

The ideal case is where the pinhole size is infinitely small. First, we consider the imaging of a point fluorescent object. Using the probability argument advanced in the text above, the instrument response is the product of the illumination and detection point spread functions. The confocal image intensity is described by

$$I=\left|h_1h_2\right|^2 \otimes f \qquad \text{(A17)}$$

where the symbols have the same meaning as before: I is intensity, h_1 and h_2 are the illumination and detection amplitude point spread functions and the squared product is convolved with the distribution function f of the fluorescent material. If the wavelength difference is neglected then the image of point object is given by

$$I(u,v)=\left|h(u,v)\right|^4 \qquad \text{(A18)}$$

Axial resolution.

The FWHM of an ideal confocal microscope in the axial direction is therefore given by the solution of

$$I(u,0)=\left(\frac{\sin\left(u/4\right)}{u/4}\right)^4=0.5 \qquad \text{(A19)}$$

which yields a value of 1.0 for $u/4$. A similar calculation to those used above gives the axial resolution as

$$FWHM = \frac{0.64\,\lambda}{n-\sqrt{n^2-NA^2}} \qquad \text{(A20)}$$

or, at low aperture,

$$FWHM = \frac{1.28n\lambda}{NA^2} \qquad \text{(A21)}$$

Lateral resolution

In this case we need to consider the solution of

$$I(0,v)=\left(2\,J_1(v)/v\right)^4=0.5 \qquad \text{(A22)}$$

This leads to v = 1.16 and to the result that

$$FWHM = \frac{0.37\lambda}{NA} \qquad \text{(A23)}$$

5. Confocal microscope with a finite detector of diameter D

In this case,

$$I = \left|h_1 h_{2eff}\right|^2 \otimes f \qquad \text{(A24)}$$

where we have introduced an *effective* emission point spread function, h_{2eff}, is given by

$$\left|h_{2eff}\right|^2 = \left|h_2\right|^2 \otimes D \qquad \text{(A25)}$$

where D represents the spatial extent of the detector pinhole. When D is infinitely small, $\left|h_{2eff}\right|^2 = \left|h_2\right|^2$ and we revert to the ideal confocal case (see Fig 4) of text. On the other hand when D is infinitely large, $\left|h_{2eff}\right|^2$ is constant and we revert to the conventional case in which

$$I = |h_1|^2 \otimes f \qquad \text{(A26)}$$

and so, for a point object,

$$I = |h_1(u,v)|^2 \qquad \text{(A27)}$$

However, a flying spot microscope such as this is not quite the same as the conventional wide-field microscope considered previously, since the resolution in this case is determined by the excitation wavelength and not the emission wavelength.

We could repeat our previous considerations of the effect of pinhole size by considering the image of a point. In this case the image is given by

$$I(u,v) = |h_1(u,v)|^2 |h_{2eff}(u,v)|^2 \qquad \text{(A28)}$$

and, if we consider, the variation along the optic axis, $v = 0$, we find

$$I(u,0) = |h_1(u,0)|^2 |h_{2eff}(u,0)|^2 = \left(\frac{\sin(u/4)}{u/4} \right)^2 |h_{2eff}(u,0)|^2 \qquad \text{(A29)}$$

and $|h_{2eff}(u,0)|^2$ is given, via equation (A25), as

$$|h_{2eff}(u,0)|^2 = \int_0^{v_p} |h_2(u,v)|^2 \, v dv \qquad \text{(A30)}$$

where v_p denotes the radius of the confocal pinhole in optical units. $|h_{2eff}(u,0)|^2$ of course, broadens from the spatially varying $\left(\frac{\sin(u/4)}{u/4} \right)^2$ with a $FWHM$ of 2x4x1.4 = 11.2 when v_p =0 to a constant when the pinhole is infinitely large. For sufficiently large defocus we may use geometrical optics to predict $|h_{2eff}(u,0)|^2$ as follows, Figure A1.

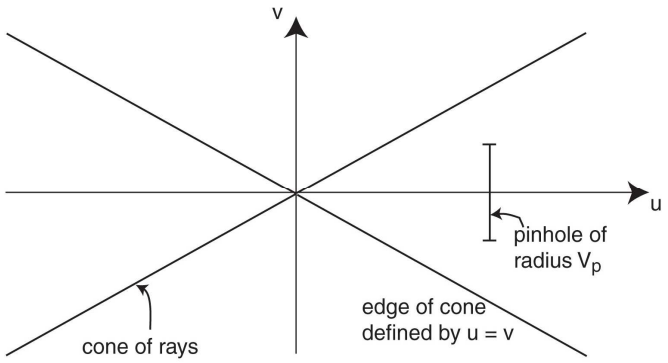

Fig A1. The geometrical optics focus.

Geometrical optics predicts that l = 1 until $v_p = u$, and thereafter $l = \left(v_p / u \right)^2$, which is the ratio of the areas. So geometrical optics predicts a $FWHM$ in optical units of $2\sqrt{2}v_p$. We may make an estimate of the variation of $FWHM$ of $\left| h_{2eff}(u,0) \right|^2$ by combining the results of wave optics, 11.2 optical units for an infinitely small pinhole, with that of geometrical optics, to predict

$$FWHM_{opt\ units} = \sqrt{(11.2)^2 + \left(2\sqrt{2}v_p\right)^2} \qquad \text{(A31)}$$

We plot this function, together with the full calculation in Figure A2.

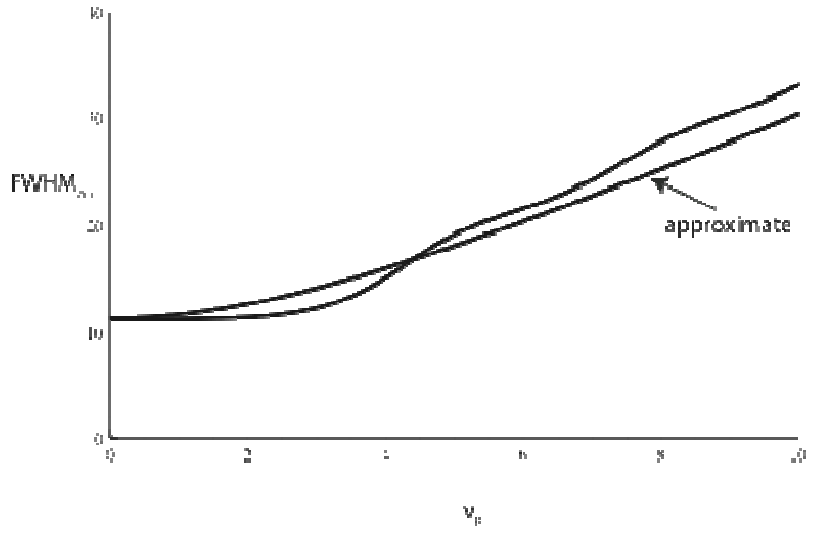

Fig A2. The variation of the $FWHM$ of $\left|h_{2eff}(u,0)\right|^2$ as a function of pinhole radius v_p together with the approximate expression of equation A31

However we must remember that we have only discussed the behaviour of $\left|h_{2eff}(u,0)\right|^2$ as a function of pinhole size. If we return to consider the *actual* image of the point, equation (A29), we find that the $FWHM$ broadens from the ideal confocal limit to the conventional limit as shown in Figure A3.

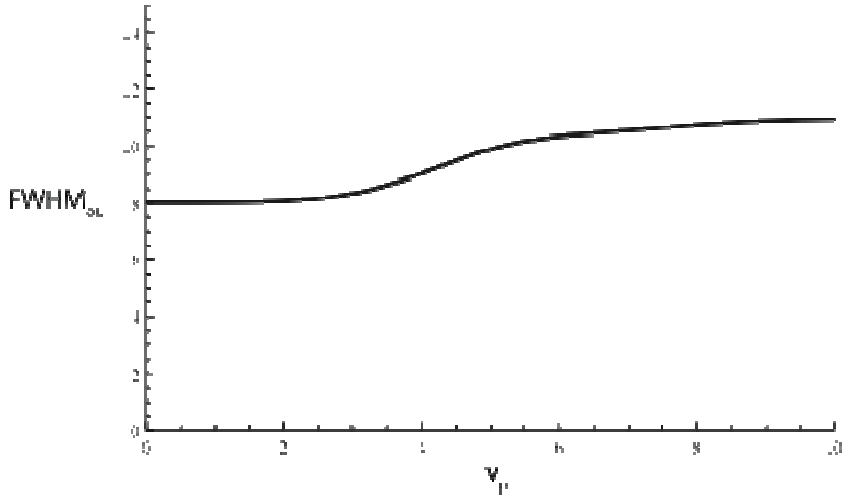

Fig A3. The variation in axial resolution of a point object as a function of pinhole size. We note that the $FWHM$ increases from 8 optical units at $v_p = 0$ corresponding to the ideal

confocal case to 11.2 optical units at large pinhole sizes corresponding to conventional imaging

6. Computation of the optical section thickness in a confocal microscope

It is most appropriate to consider a thin fluorescent sheet in this context and to consider the variation of signal as the sheet in translated axially through focus {Wilson, 1989 – Optical Sectioning in confocal fluorescent microscopes, *J. Microscopy*,**154**, 143-156.]. Computer calculation is required in this case but, again a simple analytic expression may be used which as can be seen from Figure A4 provides adequate over an appropriate range of pinhole sizes. The approximate fit may be expressed in optical units as

$$FWHM_{opt\ units} = 2\sqrt{(4.181)^2 + (1.12v_p)^2} \qquad \text{(A32)}$$

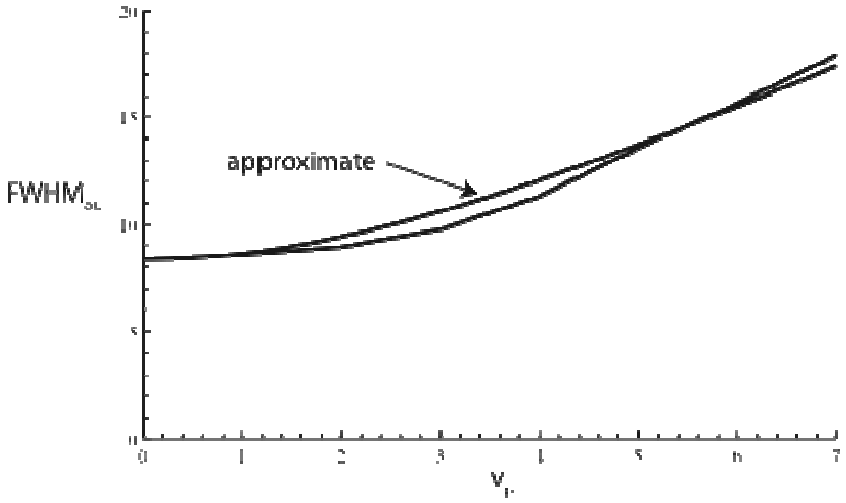

Fig A4. The variation of $FWHM$ in optical units of the signal detected as a thin fluorescent sheet is moved axially through focus as a function of pinhole diameter measure in optical units. The full calculation is compared with the approximation of equation (A32).

The results have been presented above using optical units. It is, of course, straightforward to convert these equations into practical units. In this context it is conventional to measure the pinhole diameter in Airy units. These units are normalised units such that one Airy unit corresponds to the diameter of the focal spot (often also called the Airy disc)

measured between the zero points. As such a pinhole diameter in D_{real} in real units corresponds to $D_{real} = \frac{1.22\lambda}{n\sin(\alpha)} AU$ where AU denotes the pinhole diameter in Airy units.

We may therefore re-cast equation (A32) in the more useful form as

$$FWHM = \frac{0.67\lambda}{n - \sqrt{n^2 - NA^2}} \sqrt{1 + AU^2} \qquad \text{(A33)}$$

where the $FWHM$ is measured in microns.

References

Amos, W.B. (1991) *Achromatic scanning system*. US Patent No. 4997.242

Amos,W.B. (2002) *Confocal optical microscope, magnifying attachment therefor and use thereof.* US Patent No.6,429,967 B1

Amos,W.B. (2003) *Scanning confocal optical microscope system*. US Patent 6,551,811 B1

Amos, W. B. & White, J.G. (1995) Direct view confocal imaging systems using a slit aperture. Chapter 25 pp 403-415 in *Handbook of Biological Confocal Microscopy IInd edition* ed. J.B. Pawley. Plenum Press

Amos,W.W. & White, J.G. (2003) How the confocal microscope entered biological research. *Biology of the Cell 95* 335-342.

Ball LM, Pope J, Howard CV, Eccles P, van Velzen D (1994) PCNA Ki-67 dissociation in childhood acute lymphoblastic leukaemia. An immunofluorescent laser confocal scanning microscopical study*. Cell Biol Int. 18(9*):869-74.

Born, ,M. & Wolf, E. (1980*) Principles of Optics*. 6th edition Cambridge University Press

Brakenhoff, G.J., van der Voort, H.T.M., van Spronsen, E.A. , Linnemans, W.A.M. & Nanninga, N. (1985) Three –dimensional chromatin distribution in neuroblastoma cell nuclei shown by confocal scanning laser microscopy. Nature 317, 748-749.

Buican, T.N. & Yoshida,T.M. (1992) Integrated Fluorescence Analysis System US Patent No. 5117466

Carlsson,K. & Aslund,N. (1987) Confocal Imaging for 3D digital microscopy. *Appl. Optics 26*, 3232-3238.

Curley, P.F. Ferguson,A.I., White,J.G. & Amos, W.B. (1992) Application of a femtosecond self-sustaining mode-locked titanium sapphire laser to the field of scanning laser microscopy. *Optical and Quantum Electronics 24, 851-859.*

Denk,W., Strickler,J.H. & Webb, W.W. (1990) 2-photon laser-scanning fluorescence microscopy. *Science 248*, 73-76.

Denk, W. & Svoboda, K. (1997) Photon Upmanship: why multiphoton imaging is more than a gimmick. *Neuron 18*, 351-357.

Dixon, A. & Amos, W.B. (2005) Apparatus and methods for Fourier spectral analysis in a scanning spot microscope. US Patent No. 6853455

Draaier,A.,Houpt,P.M. (1988) A standard video rate laser scanning confocal reflection and fluorescence microscope. *Scanning, 10,* 139-145.

Freed,J.J. & Engle,J.L. (1962) Development of the vibrating mirror flying spot microscope for ultraviolet spectrophotometry . *Ann. N.Y. Acad. Sci. 97. Scanning Techniques in Biology and Medicine* 412-430.

Goldstein,S.R., Hubin,T.,Rosenthal,S. & Wahburn,C. (1990) A confocal video-rate laser beam scanning microscope with no moving parts. *J. Microscopy 157*, 29-38.

Herman, B. & Tanke H. (1998*) Fluorescence Microscopy* Springer.

Inoue,S. (1989) Foundations of confocal scanned imaging in light microscopy, pp 1-13 in *The Handbook of Biological Confocal Microscopy* ed. J.Pawley IMR Press Madison.

Juškaitis,R. and T. Wilson (1999) Method for characterising longitudinal chromatic aberration of microscope objectives using a confocal optical system *J. Microscopy*, *195*, 17-22,

Kirby ,P.A., Naga,K.M. Nadella,S. and Silver,R.A. (2010) A compact acousto-optic lens for 2D and 3D femtosecond based 2-photon microscopy*. Optics Express, Vol. 18, Issue 13*, pp. 13720-13744

Masters, B. (1996) editor. Selected Papers on Confocal Microscopy. *SPIE Milestone Series. ,Volume 131.*

Matsumoto, B. (2002) editor. *Methods in Cell Biology. 70, Cell Biological Applications of Confocal Microscopy IInd edition.* Academic Press.

Minsky,M. (1998) Memoir on inventing the confocal scanning microscope. *Scanning 10* 128-138.

Murray,J. (1998) Evaluating the performance of fluorescence microscopes. *J.Microscopy. 191,*128-134.

Oldenbourg, R., Terada,H., Tiberio,R. And Inoue,S. (1993) Image sharpness and contrast transfer in coherent confocal microscopy. *J. Microscopy, 172*, 31-39.

Pawley, J.B. (2006) editor. *Handbook of Biological Confocal Microscopy. IIIrd edition.* Springer.

Petran,M., Hadravsky,J.B. ,Kucera,R. & Boyde,A. (1985) *Proc. Royal Microscopical Society, 20,* 125-129.

Reichelt S and Amos WB. (2001) SELS: a new method for laser scanning microscopy of live cells. Microscopy & Analysis November 2001, 9-11.

Roberts,F. & Young, J.Z. (1952) The flying spot microscope*. Proc. Inst. Electrical Engineers*

99, 747-757.

Sharafutdinova,G. Holdsworth,J. & van Helden D. (2009) Improved field scanner incorporating parabolic optics. *Appl. Optics 48,* 4389-4396.

Sheppard,C.J.R. (1980) Scanning optical microscope*. Electronics and Power Feb* . 166-172

Sheppard,C.J.R. (1990) 15 Years of Scanning Optical Microscopy at Oxford. *Proc. Roy. Microsc. Soc. 25,* 319-321

Sheppard,C.J.R. & Choudhry (1977) Image formation in the scanning microscope. *Optica Acta 24,* 1051-1073

Smith, F.H. (1972) A laser-illuminated scanning microinterferometer for determining the dry mass of living cells. *Microscope 20*, 153-160.

Schmidt,W., Mueller,G., Weber,K. & Wilke,V. (1983) Method and apparatus for light-induced scanning microscope display of specimen parameters and of their distribution. *U.S. Patent 4,407,008.*

Singer, S.J., Ball, E.H. , Geiger, B. & Chen,W.T. (1982) Immunolabelling studies of cytoskeletal associations in cultured cells. Organisation of the Cytoplasm. Cold Spring Harbor Symposia on Quantitative Biology 46, 303-316.

Stelzer,E.H.K. & Wijnaendts-van-Resandt,R.W. (1990) Optical cell splicing with the confocal fluorescence microscope: microtomoscopy. Chapter 7 pp 199-212 in *Confocal Microscopy* Wilson, T. editor. Academic Press.

Stelzer,E.H.K. (1995)The intermediate optical system of laser-scanning confocal microscopes. Chapter 9, pp 139-154 in *Handbook of Biological Confocal Microscopy IInd edition* ed. J.B. Pawley. Plenum Press

Tanaami,T.,Otsuki,S., Tomosada,N., Kosugi,Y., Shimizu,Y. & Ishida,H. (2002) High speed 1-frame/ms scanning confocal microscope with a microlens and Nipkow disks. *Appl.Optics. 41,* 4704-4708.

Tolansky,S. (1970) *Multiple-beam interference microscopy of metals.* Academic Press, London, New York.

Toomre , D. & Pawley, J.B. (2006) Disk scanning confocal microscopy. Chapter 10 pp 221-238 in Handbook of Biological Confocal Microscopy 3rd Edition edited J. B. Pawley. Springer

Tsien, R.Y. & Bacskai, B.J. (1995) Video-rate confocal microscopy . Chapter 29 pp 459-478 in

Handbook of Biological Confocal Microscopy IInd edition ed. J.B. Pawley. Plenum Press

Tsien,R.Y. , Rink, T.J. & Poenie, M. (1985) Measurement of cytosolic free calcium in individual small cells using fluorescence microscopy with dual excitation wavelengths. *Cell Calcium 6,* 145-157.

Tsien, R.Y. & Waggoner, A. (1995)Fluorophores for confocal microscopy. Chapter 16 pp 267-279 in *Handbook of Biological Confocal Microscopy IInd edition* ed. J.B. Pawley. Plenum Press

Wang,E., Babbey,C.M. & Dunn, K.W. (2005) (Performance comparison between the high-speed Yokogawa spinning disk confocal system and single-point confocal systems. J.Microscopy, 218, 148-159.

White, J.G. (1987) Confocal Scanning Microscope. *UK Patent Application* 2 184 321A

White , J.G. & Amos, W.B. (1987) Confocal microscopy comes of age. *Nature, 328*, 183-184

White, J.G. , Amos, W.B. & Fordham, M. (1987) An evaluation of confocal and conventional imaging of biological structures by fluorescence light microscopy. *J. Cell Biol. 105*, 41-48.

Wilson T. 1989. Optical sectioning in confocal fluorescent microscopes. *J Microsc 154:* 143–156.

Wilson, T. (1990) editor. *Confocal Microscopy* Academic Press.